琉球大学学術リポジトリ

パネル上の機能系のための効果的な結晶化によるSiおよびInSb薄膜の電気的特性に関する研究

メタデータ	言語:
	出版者: 琉球大学
	公開日: 2018-06-22
	キーワード (Ja):
	キーワード (En):
	作成者: Koswaththage, Charith Jayanada, コスワッタゲー, チャリット ジャヤナダ
	メールアドレス:
	所属:
URL	http://hdl.handle.net/20.500.12000/41489

Doctoral Dissertation of Engineering

Research on the Electrical Properties of Si and InSb Thin Films by Effective Crystallization for Functional System on Panel

March 2018

by

Koswaththage Charith Jayanada

Material, Structural and Energy Engineering

Graduate School of Engineering and Science

University of the Ryukyus

Doctoral Dissertation of Engineering

Research on the Electrical Properties of Si and InSb Thin Films by Effective Crystallization for Functional System on Panel

March 2018

by

Koswaththage Charith Jayanada

Material, Structural and Energy Engineering
Graduate School of Engineering and Science
University of the Ryukyus

Supervisor: Prof. Takashi Noguchi

We, the undersigned, hereby, declare that we have read this thesis and we have attended the thesis defense and evaluation meeting. Therefore, we certify that, to the best of our knowledge this thesis is satisfactory to the scope and quality as a thesis for the degree of Doctor of Engineering in Material, Structural and Energy Engineering, Graduate School of Engineering and Science, University of the Ryukyus.

THESIS REVIEW & EVALUATION COMMITTEE MEMBERS

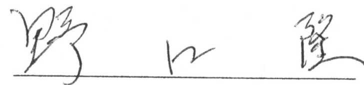

(Chairman) Takashi Noguchi

(Committee) Akira Higa

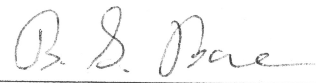

(Committee) Byung-Seong Bae

Table of Contents

Table of Contents ……………………………………………………………………………………..ii

List of Figures ………… …………………………………………………………………….. iv

List of Tables ………………………………………………………………………………….. v

Abstract ……………………………………………………………………………………… vi

1. **Introduction**

    1.1. Background ………………………………………………………………………. 1

    1.2. Structure of the dissertation ……………...…………………..……………….…………….. 2

2. **Thin Si film for Photosensor Applications**

    2.1. Introduction……………………………………………………………………… 4

    2.2. Crystallinity evaluation by BLDA ………………….…………………………..…….. 6

    2.3. Crystallinity evaluation by Spectroscopic Ellipsometry (SE) …………………………..…….. 7

    2.4. Crystallinity evaluation by TEM ……………………………..…………………….……… 8

    2.5. Crystallinity evaluation by AFM ……………………………..……………………….… 10

    2.6. Photoconductivity of poly-Si thin film ………………………………..……………….…… 13

    2.7. Effect of H_2 Annealing …………………………..………………………………...…… 16

    References …………………………………………………………………...……. 19

3. **Multilayer Structure for Photosensor Applications**

    3.1. Introduction ………………………………………………………………………… 21

    3.2. Photoelectric characteristics ……………………………………………………….….. 24

    3.3. Simulation Results ………………………………..……………………………..…. 26

    3.4. Reflectivity Analysis of Multilayer Structure ……………………………………..………… 28

    3.5. XRD Analysis of Multilayer Structure …………………………………..………………… 30

    References ………………………………………………………………………… 32

4. **Vacuum Evaporated InSb film for Magnetic Sensor Applications**

    4.1. Introduction ………………………………………..…………………..……………… 33

    4.2. Crystallinity evaluation of Furnace Annealed InSb films by TEM …..…………..………… 35

    4.3. Crystallinity evaluation of Furnace Annealed InSb films by Spectral Transmittance ………… 36

    4.4. Sheet resistance measurement of Furnace Annealed InSb films …………..………………..… 38

4.5. Electron Hall mobility measurement for Furnace Annealed InSb films ……………………….….. 39
4.6. Hall mobility measurement of Rapid Thermal Annealed InSb films …………….…………… 40
4.7. Dependency of Hall mobility on RTA annealing time for InSb on glass substrate………… 41
4.8. Crystallinity evaluation of Rapid Thermal Annealed InSb films by reflectance spectroscopy .. 43
4.9. In:Sb ratio by EDS analysis ……………………………..…………………..…….….… 45
References ……………………………………………………………………………….… 46

5. **Sputtered InSb film for Magnetic Sensor Applications**
5.1. Introduction…………………………………………………………………………..………. 47
5.2. Crystallinity evaluation of Rapid Thermal Annealed InSb films by reflectance spectroscopy … 48
5.3. Surface morphology of InSb films after RTA by SEM, AFM ……………………………..… 50
5.4. Electron Hall mobility of InSb films after RTA ……………………………….…………… 54
5.5. InSb composition ration by EDS analysis after RTA ………………………………………… 55
5.6. Crystallinity evaluation of BLDA applied InSb films by spectral reflectance ………………… 56
5.7. Crystallinity evaluation of BLDA applied InSb films by XRD…………………..………………… 57
5.8. Surface morphology of InSb films after RTA by SEM, AFM …………………….………… 58
5.9. InSb composition ration by EDS analysis ……………………………………………………… 59
5.10. Electron Hall mobility of InSb films after BLDA ………………………………….……. 60
5.11. De-gas analysis of InSb films ……………………….…………………………………... 61

6. **Application as multifunctional TFT system on panel** ……………………………….……… 65
7. **Summary and Conclusion** ………………………………..……….……………………….…… 66

Acknowledgments ………………………………..…………………………………..……..…… 67
List of Publications ………………………………..………………………………….……….…… 68

List of Figures

2.1 Extinction coefficient spectra obtained by SE of the Si films before and after the BLDA …………..... 7

2.2 TEM images of the Si films after BLDA at (a) 4, (b) 5, and (c) 6W. ………………………………… 9

2.3 Surface morphologies obtained by AFM of the Si films before and after the BLDA. ……………….. 12

2.4 (a) Dark currents of the Si films before and after the BLDA …………………………………………. 13

2.4 (b) Photocurrents of the Si films before and after the BLDA ………………………………………… 14

2.5 Photocurrents of the Si film after the BLDA at 6W under red, green, and blue light exposures. ……. 15

2.6 (a) Dark conductivities of the Si films before and after H_2 annealing ……………………………… 16

2.6 (b) Photoconductivities of the Si films before and after H_2 annealing …………………………… 17

2.7 Photosensitivity ratios ($\sigma_{photo}/\sigma_{dark}$) biased at 20 V before and after the BLDA and H_2 annealing ….. 18

3.1 Proposed highly sensitive photosensor structure with multi-layer structure as a TFT system. ……… 23

3.2 (a) Photocurrent characteristics before and after H_2 annealing (b) Photoconductive characteristics compared to BLDA 4 W under white light exposure of 100 mW/cm^2 ……………….……………. 24

3.3 Light absorption rate to the wavelength of multi-layer structure with Ti back-reflection layer …..… 27

3.4 (a) Reflectivity analysis results of single layer ……………………………………………………… 28

3.4 (b) Reflectivity analysis results of multi-layer structure with Ti back-reflection layer…………….…… 29

3.5 XRD analysis results of Si film with Ti back-reflection layer (1 cm x 1 cm) ……………………… 30

3.6 XRD analysis results for Ti layer on glass (2.5 cm x 1.8 cm) ……………………………………… 31

4.1 TEM images of the InSb films on (a) mica and (b) glass substrates after FA ……………….…… 35

4.2 (a) Transmittance of 1 μm thick InSb films on mica substrates after FA ……………………….… 36

4.2 (b) Transmittance of 1 μm thick InSb films on glass substrates after FA …..………………………... 37

4.3 Sheet resistance of InSb before and after FA …………...……..………………….……........…… 38

4.4 Electron Hall mobility of InSb before and after FA …………….……………………………….…. 39

4.5 Dependency of electron Hall mobility on RTA annealing temperature for InSb on glass substrate .. 40

4.6 Dependency of Hall mobility on RTA annealing time for InSb on glass substrate…………………… 42

4.7 Extinction coefficient of crystalline InSb ……………………………………………………..……. 43

4.8 Reflectance spectra of 1 μm thick InSb films after RTA at 520°C ………………………………… 44

5.1 Reflectance of 300 nm thick sputtered InSb films before and after RTA …………………………… 49

5.2 Surface morphology of sputtered InSb films before and after RTA……………………….……... 53

5.3 Dependence of electron Hall mobility on RTA temperature ……………………………………… 54

5.4 Reflectance of sputtered InSb films before and after BLDA ………………………………………. 56
5.5 XRD analysis results of InSb film after BLDA ……………………………………………………. 57
5.6 Surface morphology of sputtered InSb films before and after BLDA ……………………………….58
5.7 Dependence of electron Hall mobility on laser power …………………………………………….. 60
5.8 (a) TDS results of InSb film for Oxygen gas ……………………………………………………… 61
5.8 (b) TDS results of InSb film for Ne gas. ………………………………………………….…….. 62
5.8 (c) TDS results of InSb film for Ar gas …………………………………………………………… 62
5.9 (a) TDS results of InSb film for In ……………………………………………………………… 63
5.9 (b) TDS results of InSb film for Sb ……………………………………………………………… 64
6.1 Integrating sensor devices with TFTs on panel …………………………………………………... 65

List of Tables

4.1 In:Sb ratio deduced from energy-dispersive X-ray spectroscopy (EDS) ..…………………………… 45
5.1 EDS analysis of InSb films after RTA….………………………………………………………….. 55
5.2 EDS analysis of InSb films after BLDA …………………………………………………………….. 59

Abstract

Effective crystallization process to realize advance multifunctional next generation System on Panel (SoP) which can integrate Si photosensors or/and InSb magnetic sensors with Thin Film Transistors (TFT) was investigated.

Thin amorphous Si (a-Si) film of 50 nm thickness was fabricated using radio frequency (RF) sputtering. The photoconductivity of poly-crystallized Si films after blue laser diode annealing (BLDA) has been measured and analyzed. As the laser power was increased from 4 to 6 W, the crystal structure changed from micro grains to laterally large grains. Photoconductivity value under the white light exposure of 100 mW/cm^2 reached as high as 8.1 x 10^{-4} S/cm for the Si film after H_2 annealing in H_2/N_2 (4%) ambient after subsequently after the BLDA at 6 W. Resultant photosensitivity ratio ($\sigma_{photo}/\sigma_{dark}$) of 94 was obtained owing to the reduction in the defects density in the Si films.

At first, highly photosensitive Si film of new structure was successfully fabricated on glass by performing semiconductor BLDA. Simulation results showed 86% increase of light absorption in red or Infra-Red (IR) region by adopting back-reflection Ti layer. Peaks from X-Ray Diffraction (XRD) analysis results showed that Si film was crystallized clearly after BLDA despite the inserted new back-reflection layer of Ti on glass. After H_2 annealing, photoconductivity for the patterned Si films of 50 nm thickness prepared by photo-lithography increased remarkably up to 3.2 x 10^{-1} S/cm from 1.2 x 10^{-4} under white light of 100 mW/cm^2. These results suggest, adopting back-reflection layer under the crystallized Si film is promising to integrate functional photosensors with TFTs on panel. Thus, thin Si film crystallized using BLDA is promising for photosensor applications in a multifunctional system on panels.

Secondary, InSb films of III-V compound material were deposited on both mica and glass substrates using thermal evaporation and were subjected to Furnace Annealing (FA) or Rapid Thermal Annealing (RTA). Crystallinity, composition and electrical properties of the films were investigated. High value of electron Hall mobility as high as 25,000 cm^2/(Vs) was obtained with the capped InSb film by keeping the In:Sb ratio after RTA at 520°C for 30 sec without adopting epitaxial growth on single crystalline substrate.

Furthermore, InSb films were deposited using r.f. sputtering and effect of various deposition conditions such as gas species (Ne or Ar), gas pressure and film thickness were investigated. Both RTA and BLDA were used to crystallize the InSb films effectively. In the case of RTA, the obtained electron Hall mobility was 1,650 cm^2/(Vs) after annealing at 500°C for 30 s. Maximum electron Hall mobility of 1,050 cm^2/(Vs) was obtained after BLDA at 4 W for the InSb film sputtered using Ar gas at the pressure of 7.0 mTorr for the InSb film of 300 nm thickness. These results suggest that InSb film after RTA or BLDE is a promising candidate for IR sensor applications.

BLDA is a promising method to crystallize both Si or InSb films not only on glass but also on flexible plastic substrates, which can be applied for the fabrication of next generation SoP by integrating the sensors with TFT system.

These results can be expected as a functional sensor for SoP, as a TFT functional system which is also applicable for future Internet on Things (IoT) devices.

概要

Si フォトセンサや InSb 磁気センサを薄膜トランジスタ（TFT）回路アレイと同一の任意のパネル上に集積可能な次世代多機能 SoP を実現するための効果的な結晶化プロセスの検討を行った。

スパッタ法を用いて厚さ 50 nm の非晶質 Si（a-Si）薄膜を作製した。青色レーザーダイオードアニーリング（BLDA）により得られた多結晶 Si 膜の状態を解析し、光伝導度を測定した。レーザー出力が 4W から 6W に増加するにつれて、結晶構造は微小粒子から横方向に大きな粒子に変化した。 6W の BLDA 後の Si 膜を H_2 / N_2（4%）雰囲気中で H_2 アニールを施したが、Si 膜中の欠陥密度の低下により、100 mW / cm^2 の白色光照射下での光導電率を測定すると、値は 8.1×10^{-4} S / cm に達し、94 の高い光感度（$\sigma_{photo}/\sigma_{dark}$）が得られた。

BLDA を行うことにより、本研究室で提案された新しい構造の高感度ポリ Si 膜をガラス上に作製することに成功した。計算シミュレーション結果、裏面反射 Ti 層を採用することにより、赤色または赤外線（IR）領域で光吸収が 86%増加することを予測された。 X 線回折（XRD）分析結果からの回折ピークから、ガラス上 Ti による裏側反射層を挿入したにもかかわらず、BLDA 後に Si 膜が明確に結晶化されたことが確認された。 続いて、H_2 アニーリング後、フォトリソグラフィーで作製した厚さ 50 nm のパターニングした Si 膜の光導電率は、100 mW / cm^2 の白色光下で 1.2×10^{-4} から 3.2×10^{-1} S / cm まで著しく増加した。これらの結果は、結晶化した Si 膜の下に裏面反射層を採用することにより、機能的な光センサとパネル上の TFT との統合が有望であることを示している。したがって、BLDA を用いて結晶化された薄膜 Si は、パネル上の多機能システムにおける光センサ用途に期待できる。

つぎに、III-V 化合物材料である InSb 膜を、真空加熱蒸着法用いてマイカ（雲母）およびガラス基板上に堆積させ、その後、InSb 膜にキャップ膜を覆い、炉アニール（FA）または急速熱アニール（RTA）を行った。膜の結晶性、組成および電気特性を調べた。単結晶基板上のエピタキシャル成長を採用せずに、520℃、30 秒間の RTA 後 In：Sb 比を維持することにより、安価な絶縁ガラス上に、多結晶化薄膜の状態で 25,000 cm^2/(Vs) の非常に高いホール移動度が得られた。

さらに、スパッタ法により InSb 膜をガラス上に製膜し、ガス種（Ne または Ar）、ガス圧力、膜厚など変化させて、RTA と BLDA の両方を用いて効果的に結晶化させた。RTA の場合、得られたホール移動度は、500℃で 30 s のアニール後に 1,650 cm^2/(Vs) であった。場合、圧力 7.0 mTorr の Ar ガスを用いてスパッタリングした厚さ 300nm の InSb 膜では、4W の BLDA により、1,050 cm^2/(Vs)の最大電子ホール移動度が得られた。これらの結果より、RTA または BLDE 後の InSb 膜は、感磁性素子や IR センサなどの用途として有望な候補と期待される。

BLDA 法は、ガラス上だけでなく、TFT システムとセンサを統合した次世代 SoP としてフレキシブルなプラスチック基板上への有効な薄膜結晶化プロセスとして有望である。

以上の結果は、今後の IoT（Internet on Things）デバイスにも適用可能な TFT 機能システム、高機能 SoP として期待される。

Chapter 1

Introduction

1.1 Background

In the information society, display and tablet devices with high performance, multi-functions got high attention with the development of semiconductor display industry. System on Panel (SoP) or System on Glass (SoG) is a technical concept which can realize high performance, multi-function and cost reduction by packing more effective circuit elements on a single display panel substrate.

To the realization of SoP, Si device capable of high-speed operation is required. Low carrier mobility of the hydrogenated amorphous silicon (a-Si:H) TFT is a major obstacle although the a-Si TFTs are used widely to drive LCD pixels. Polysilicon (poly-Si) achieved by crystallizing a-Si film on the glass is an effective solution to this problem. Currently, there are panel products which have driving circuits formed on the glass. Without limiting to the driving circuits, lateral PIN photodiode can be also added to the touch panel sensor, because it can be fabricated in the same process and expected to improve the cost reduction.

Making the photosensor on the glass panel, the light absorbing layer is required to be at the thickness of the same 50 ~ 100 nm in terms of production process of the Si TFTs. However, most of the light would be transmitted because Si film is very thin. Thus, it is not possible to obtain sufficient photosensitivity. In order to obtain a high optical sensitivity even with a small light absorption, producing a poly-Si film with a high carrier mobility and long lifetime with increased light absorption is required. Conventionally, Excimer Laser Annealing (ELA) method, Metal Induced Crystallization (MIC) method and Solid Phase Crystallization (SPC) methods are used to the crystallization tools of Si films.

Recently, BLDA technique, a valid high-quality crystallization method that can accurately control the Si crystallinity i.e the grain size in the Si film, has been reported in this laboratory. In this study, BLDA was used to the crystallization of Si film, in order to obtain a high light sensitivity with a thin film by making poly-Si film with a smooth surface with controlled grain sizes. To improve the photosensitivity, hydrogen annealing at low temperature was performed after BLDA.

Indium Antimonide (InSb) is a material with high carrier mobility, which is widely used in magnetic field sensors, thermal imaging cameras and infrared detectors. Conventionally, InSb layer with high carrier mobility is produced by epitaxial growth on single-crystal substrate using expensive process such as molecular beam epitaxy (MBE). Fabricating InSb film on glass substrate has high potential from the perspective of low-cost process and functional applications.

Integrating sensor devices with TFTs on panel can realize futuristic high-end multifunctional systems with cost reduction. In this dissertation I targeted two types of sensor devices, photosensor and magnetic sensor.

1.2 Structure of the dissertation

This dissertation consists 7 chapters:

Chapter 1: Introduction

Chapter 2: Thin Si film for Photosensor Applications
(Journal Article [1], International Conference Article [2])

Chapter 3: Multilayer Structure for Photosensor Application
(Journal Article [1,2], International Conference Article [7])

Chapter 4: Vacuum Evaporated InSb film for Magnetic Sensor Application
(Journal Article [3], International Conference Article [13])

Chapter 5: Sputtered InSb film for Magnetic Sensor Applications
(Journal Article [3], International Conference Article [14,15,16])

Chapter 6: Application as Multifunctional TFT System on Panel

Chapter 7: Summary and Conclusion

Chapter 2

This chapter is mainly focused on effective crystallization of thin Si film with BLDA and subsequent H_2 annealing. In the purpose of photosensor application, photoconductivity of annealed Si film was investigated. With the increase of laser power from 4 to 6 W, the crystal structure changed from micro grains to large grains, and correspondingly the photoconductivity increased. After H_2 annealing for the Si films in H_2/N_2 (4%) ambient at 450°C, photosensitivity ratio ($\sigma_{photo}/\sigma_{dark}$) of 94 was obtained under white light exposure of 100 mW/cm^2 after the BLDA at 6 W owing to the reduction in the defects density in the Si films.

Chapter 3

This chapter is mainly focused on effective crystallization of thin Si film with BLDA and subsequent H_2 annealing with the adoption of proposed multilayer structure [13]. By adopting metal back-reflection layer, simulation results show 86% increase of light absorption in red or IR region. Peaks from XRD results showed that Si film was crystallized clearly after BLDA in spite of the inserted new back-reflection layer of Ti. All the process for photoconductive film was performed using RF sputtering and vacuum evaporation without adopting Chemical Vapor Deposition (CVD). After H_2 annealing, photoconductivity for the

patterned Si films of 50 nm thickness increased remarkably up to 3.2×10^{-1} S/cm from 1.2×10^{-4} under white light of 100 mW/cm^2.

Chapter 4

In this chapter, crystallinity, composition and electrical properties of thin InSb films were investigated. Films were deposited on both mica and glass substrates using thermal evaporation and subjected to FA or RTA. High electron Hall mobility as high as 25,000 cm^2/(Vs) was obtained with the capped InSb film by keeping the In:Sb ratio after RTA at 520°C for 30 sec or longer without adopting epitaxial growth on glass.

Chapter 5

This chapter is focused on effective crystallization of thin InSb films deposited by RF sputter and annealed with BLDA and RTA. Crystallinity, electron Hall mobility and surface morphology of annealed InSb film were investigated for the purpose of magnetic sensor application. Furthermore, effect of various deposition conditions such as gas type (Ne, Ar), gas pressure and film thickness were investigated. Both RTA and BLDA were used to crystallize the InSb films effectively. In the case of RTA, the obtained electron Hall mobility was 1,650 cm^2/(Vs) after annealing at 500°C for 30 s. Maximum electron Hall mobility of 1,050 cm^2/(Vs) was obtained with the InSb film sputtered with Ar gas at the pressure of 7.0 mTorr for the 300 nm thick film after BLDA at 4 W.

Chapter 6

This chapter is focused on new application of the obtained results as a multifunctional TFT system on panel.

Chapter 2

Thin Si film for Photosensor Applications

2.1. Introduction

Multifunctional flat panel displays are now demanded with the rapid spread of smart phones and tablet devices owing to their low cost, low power consumption, and downsizing capabilities. Thin-film lateral structured photosensors are required in flat panel display systems with optical functions such as brightness control against ambient illuminance or touch panel sensors [1–4]. Several studies of thin-film photodiodes or phototransistors have been reported [5–10]. Thin-film transistors (TFTs) and photosensors are formed on the identical substrates by adopting a simultaneous or compatible fabrication process to realize a multifunctional system on panels (SoP) [11, 12].

In general, the channel layer thickness of polycrystalline Si (poly-Si) TFTs is designed to be between 50 and 100 nm. At this thickness, the light absorption of Si films is poor owing to the loss of light energy through transmittance. Therefore, it is important to develop sensitive photosensors even for red or IR light. A new structure of sensitive pin photosensors with a micro grained Si film simultaneously fabricated with high-performance TFTs on a panel has been proposed and reported [13].

As a crystallization tool, blue multi-laser diode annealing (BLDA) is a promising annealing tool, which is expected for use in low-temperature poly-Si (LTPS) fabrication [14–20] Si films with controlled micro- to large-grains are formed reproducibly with a smooth surface by adopting scanning BLDA, although their grain size can be hardly controlled by pulsed excimer laser annealing (ELA) [21,22] Si films of various grain structures formed by BLDA should be studied to realize higher-performance TFT systems with functional photosensors.

On the other hand, to realize SoP on flexible plastic substrates, a low-temperature deposition method must be used. RF sputtering is a method that can achieve a higher deposition rate at room temperature for both undoped and doped semiconductors as well as for conducting and nonconducting materials. For sputter deposition, Ar gas is normally used as the sputtering gas. Ar atoms attack the Si target and are incorporated into the Si film. If a laser beam of high power is irradiated onto a Si film, the surface roughness of the film degrades owing to the rapid release of the incorporated atoms. A smooth surface can be obtained by sputtering using He gas, as the He atom has a small atomic radius [23]. However, sputtering using He gas markedly decreases the sputtering efficiency i.e. lowers the deposition rate, which affects the deposition rate. Sputtering using Ne gas can achieve a comparative deposition rate with that using Ar gas. Since the

atomic radius of the Ne atom (r = 1.2 Å) is close to that of the Ar atom (r = 1.6 Å), sputtering using Ne gas is expected to be effective for achieving a smooth surface after subsequent laser annealing. Therefore, we have utilized Si films deposited by sputtering using Ne gas as precursor films for BLDA.

In this chapter, the photoconductivity of Si films after BLDA has been investigated for photosensor applications. The relationships between the laser power, crystal structure, and photoconductivity were clarified, and the effect of H_2 annealing on the photosensitivity of Si film was also clarified. We suggest the potential of Si films after BLDA for photosensor applications.

2.2. Crystallization by BLDA

Amorphous Si (a-Si) films of 50 nm thickness were deposited using RF sputtering at room temperature using a semi intrinsic Si target (5–10 Ωcm). Deposition was carried out under the optimized conditions of Ne gas at an RF power of 450W. The gas flow rate and working pressure were controlled at 13 sccm and 1.4 mTorr, respectively. Buffer layers of SiO_2 films of 50 nm thickness were pre-deposited to protect the Si films from impurities in the glass substrate.

Subsequently, the deposited thin Si films were annealed using semiconductor blue laser diodes of 445 nm wavelength in a continuous wave mode. The samples were placed on a high-precision computer-controlled x–y stage, and a beam of 600 × 2.4 μm^2 with a top-flat power profile along the long axis was irradiated at a scanning speed of 500 mm/s in atmospheric ambient [14, 16]. The laser power was controlled between 4 and 6 W, which corresponds to a laser density between 1.3 and 2.0 J/cm^2. The thickness (d), refractive index (n), and extinction coefficient (k) of the Si films were measured by spectroscopic ellipsometry (SE; SOPRA ES4G). Transmission electron microscopy (TEM) was also performed to observe the crystal grain structure of the Si films after the BLDA. Atomic force microscopy (AFM) was performed to observe the surface smoothness. Some of the samples were annealed in H_2/N_2 (4%) ambient at 400 or 450°C for 1 h. Al electrodes were deposited on Si films using thermal evaporation for current–voltage (I–V) measurement. Each electrode was 8 × 8mm^2 with a gap of 1mm for the light absorption area. The photocurrent and dark currents of the Si films before and after the BLDA and H_2 annealing were measured using a solar simulator (HMT MFS-PV-Basic) to measure the photoconductivity and the photosensitivity was deduced, i.e., $\sigma_{photo}/\sigma_{dark}$, where σ_{photo} is the photoconductivity under white light exposure and σ_{dark} is the conductivity in the dark. Furthermore, red, green or blue light spectrum was irradiated selectively onto the Si films, and the photocurrent was measured.

2.3. Crystallinity evaluation by Spectroscopic Ellipsometry (SE)

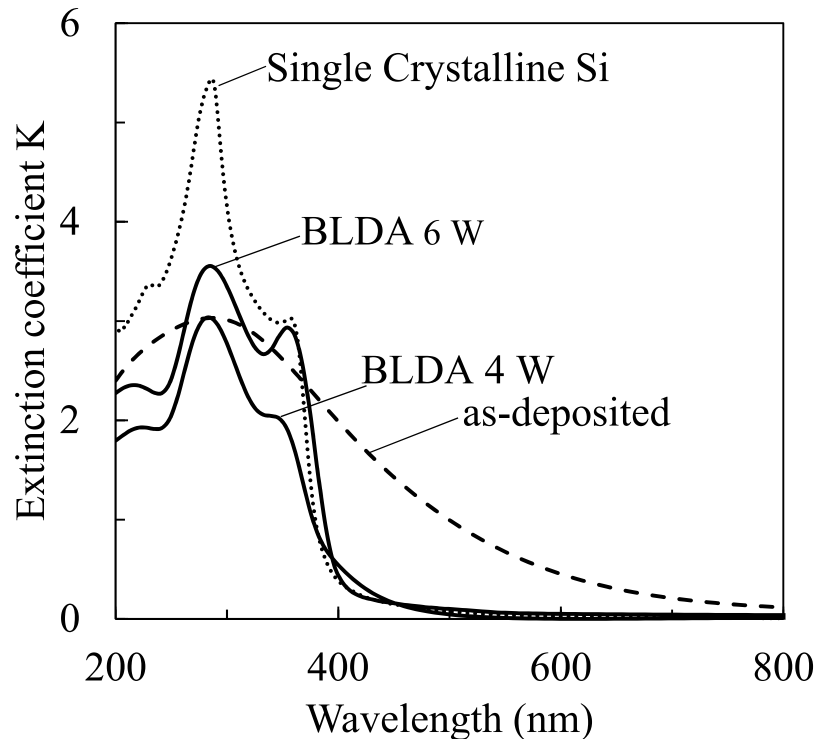

Fig. 2.1 Extinction coefficient spectra obtained by SE of the Si films before and after the BLDA (Journal Article [1]).

Figure 2.1 shows the extinction coefficient spectra obtained by the SE for the Si films before and after BLDA. For the as-deposited a-Si film, a broad peak was confirmed. On the other hand, after performing the BLDA of 4 W, the peak at a wavelength of approximately 280 nm was sharpened, and a small shoulder at approximately 360 nm was newly observed. With the increase in laser power to 6 W, the peak remains the same shape, and the shoulder became clearer. For single-crystal Si, distinct two peaks were observed there. Here, the peaks at approximately 280 and 360 nm correspond to the absorption peaks for the band-to-band transitions of electrons in crystal Si, which are called E_1 and E_2 peaks whose energies are 4.4 and 3.4 eV, respectively [24, 25] As a result, the crystallinity of the Si films can be evaluated qualitatively from the sharpness of the peaks in the waveform. Therefore, these results indicate a band structure was formed by performing the BLDA and the crystallinity depends on the laser power, and the crystallinity became closer to that of single-crystal Si.

2.4. Crystallinity evaluation by TEM

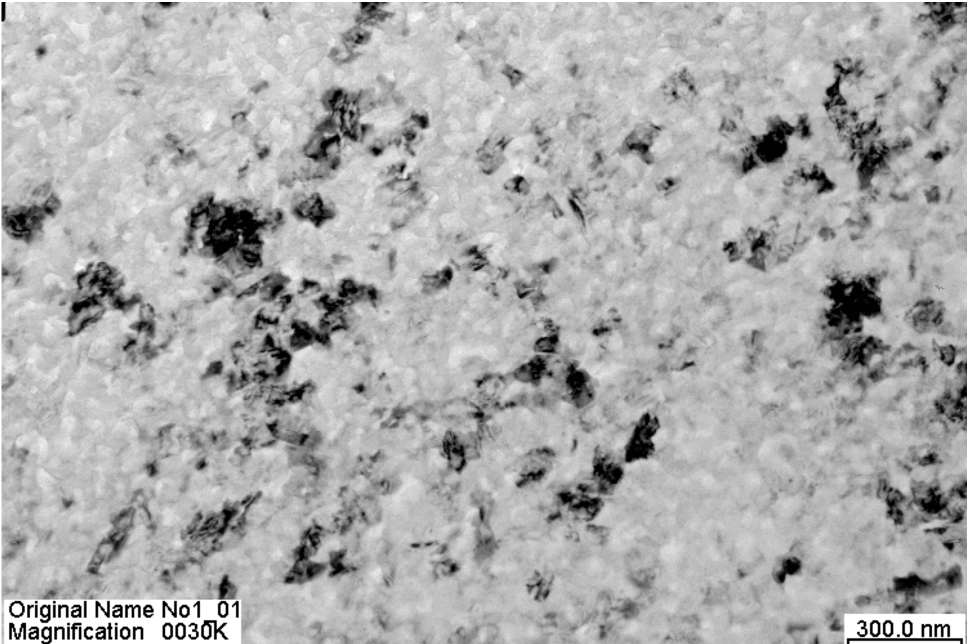

(a)

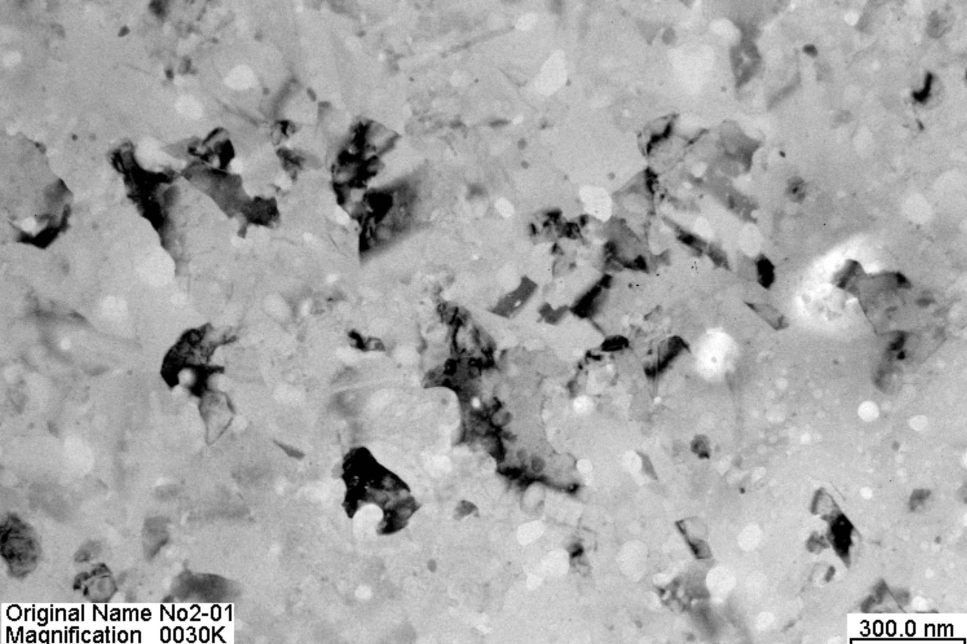

(b)

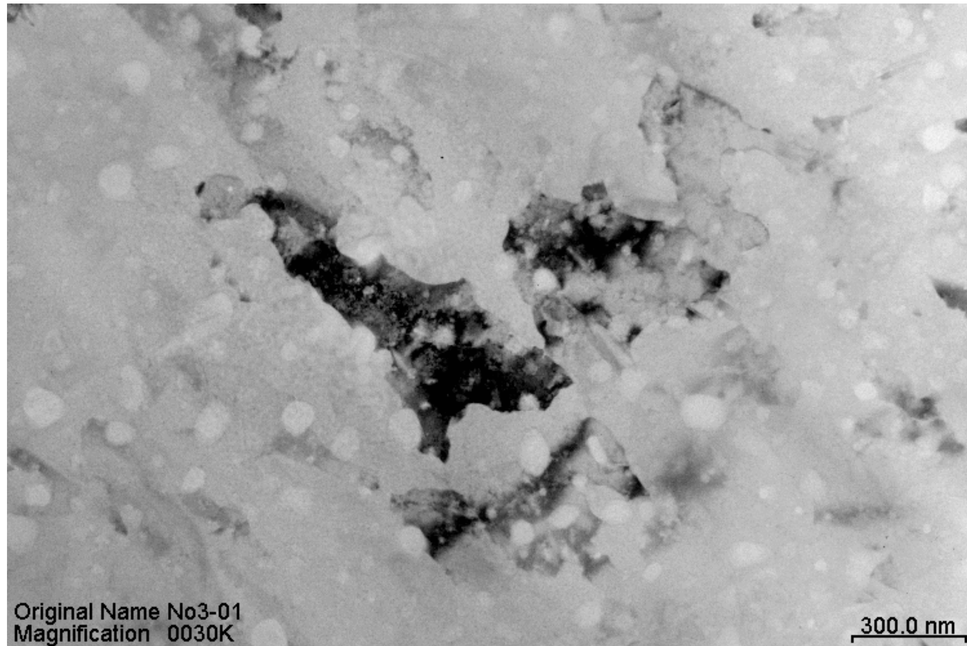

(c)

Fig. 2.2 TEM images of the Si films after BLDA at (a) 4 W, (b) 5 W, and (c) 6 W (Journal Article [1]).

Figure 2.2 shows TEM images of the Si films after the BLDA at (a) 4 W, (b) 5 W, and (c) 6 W. As a result of the BLDA, the a-Si films were poly-crystallized efficiently and stably. Rather small grains or micro grains of approximately 50 nm in diameter were formed for the Si film after the BLDA at 4 W, as shown in Fig. 2.2(a). Because its grains are small, the Si film is suggested to have crystallized in the solid phase at a high temperature under uniform rapid heating [27–29]. The grain size increased with an increase in the laser power. For the Si film after the BLDA at 5 W, grain sizes roughly ranging from 100 to 150 nm were obtained. From the SE results, larger grains are speculated to be formed when the laser power is increased to 6 W, as in the case of CVD film [16]. Thus, considerably large Si grains were observed, as shown in Fig. 2.2(c). In the cases of the BLDA at 5 W and 6 W, it is considered that large grains might be obtained by the liquid phase crystallization of the Si films. It is speculated that the volume ratio of crystalline to amorphous, i.e., the crystallinity, increases with the laser power. Therefore, the crystallinity became higher and the photoconductivity increased owing to the increase in the carrier lifetime and the mobility.

2.5. Crystallinity evaluation by AFM

Figure 2.3 shows the surface morphologies obtained by AFM for the Si films before and after BLDA. The observed region is 10 × 10 μm^2.

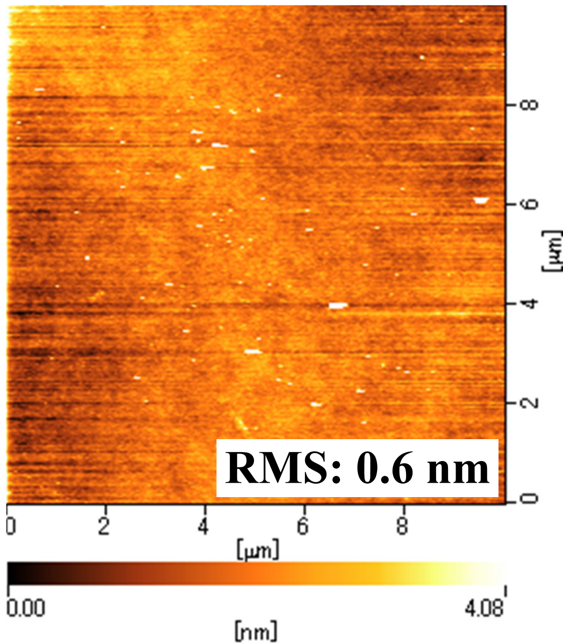

(a) As deposited

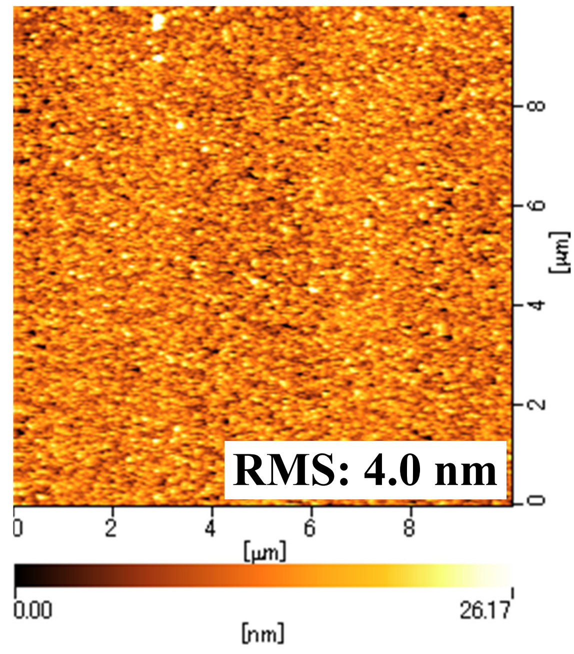

(b) BLDA at 4 W

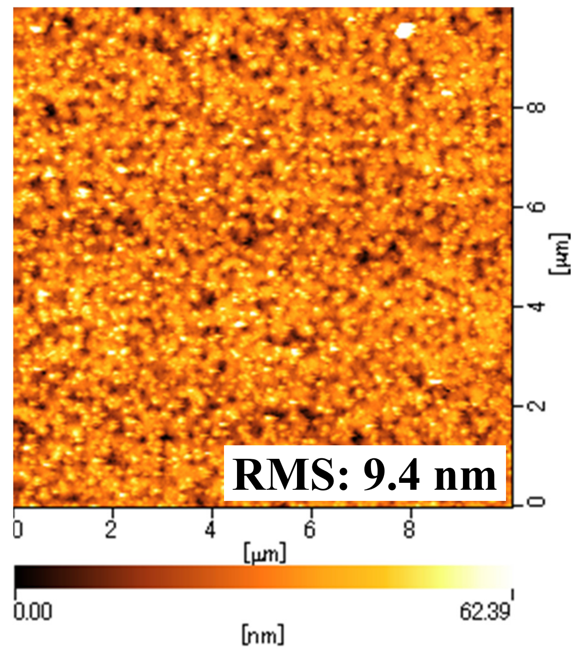

(c) BLDA at 5 W

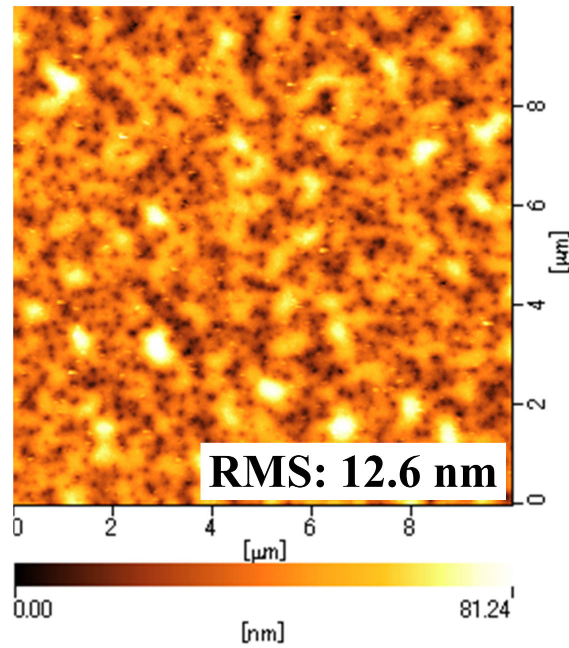

(d) BLDA at 6 W

Fig. 2.3 Surface morphologies obtained by AFM of the Si films after BLDA (Journal Article [1]).

The surface roughness slightly increased due to the crystallization after the BLDA. The root mean square (RMS) values of the surface roughness were less than 13 nm for the Si film after the BLDA at 6 W [30]. This surface roughness is lower than that after ELA, where the surface roughness sometimes becomes as high as the film thickness itself. Because the surface of the Si films after the BLDA is smooth, the recombination of carriers at the surface was suppressed and it is speculated that the photosensitivity increased.

2.6. Photoconductivity of poly-Si thin film

Figure 2.4. (a) shows the dark currents of the Si films before and after BLDA. *I–V* characteristics were measured in the dark ambient. Compared with the as-deposited Si film, the Si films after BLDA showed a reduction in dark current. This result indicates that the conduction mechanism was speculated to change from a hopping-like conduction to activated conduction of poly-crystalline Si [26]. For the as-deposited Si films deposited by sputtering without hydrogen annealing, the conduction mechanism was speculated to be, in general, rather variable-range hopping conduction. After the BLDA, as a result of crystallization, a band gap was clearly formed, and the density of states related to the defects inside the gap decreased drastically, and the conduction mechanism changes to a rather activated conduction even without performing hydrogenation. In general, the conductivity value undoped a-Si just before crystallization is higher than that for the activated conduction of undoped poly-Si at room temperature [26].

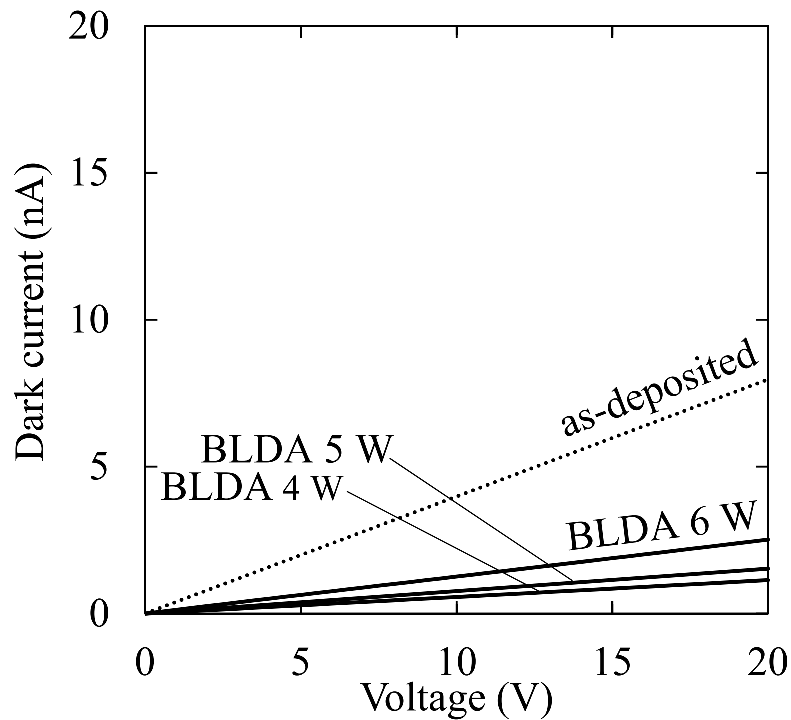

Fig. 2.4 (a) Dark currents of the Si films before and after the BLDA (Journal Article [1]).

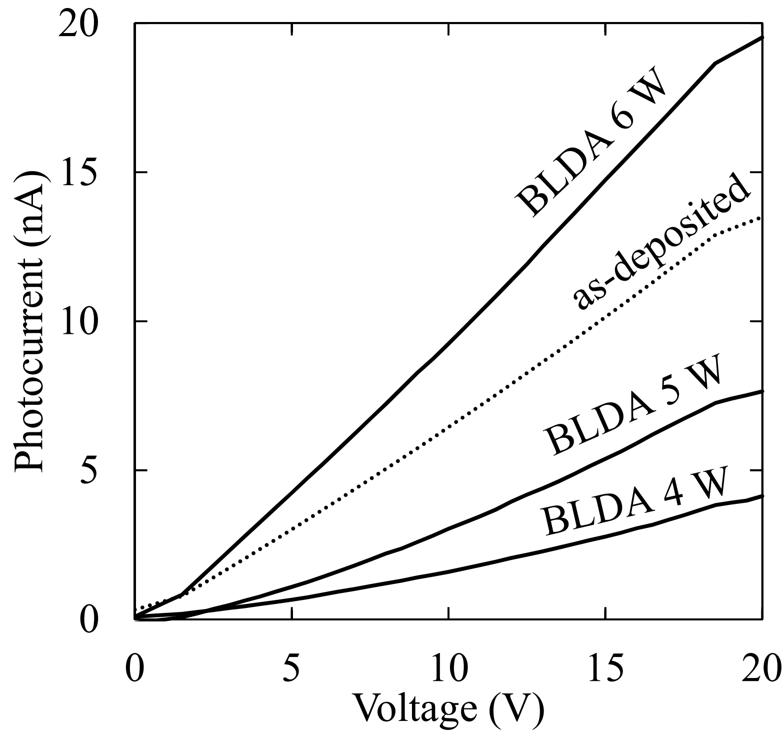

Fig. 2.4 (b) Photocurrents of the Si films before and after the BLDA (Journal Article [1]).

Figure 2.4(b) shows the photocurrents of the Si films before and after the BLDA. *I*–*V* characteristics are measured under white light exposure of 100mW/cm^2. The photocurrent increased with an increase in the laser power. The photocurrents of the Si films after the BLDA were smaller than that of the as-deposited Si film except at 6 W. However, the photocurrent of the Si film after the BLDA at 6 W markedly increased and became higher than that of the as-deposited Si film. At 6 W, it is considered that the photocurrent increased owing to the improvement in the crystallinity. On the other hand, the dark current of the as-deposited Si film was rather high, probably, due to the effect of hopping based conduction, and it is considered that the photocurrent became slightly higher than the dark current. The dark current of the Si films after the BLDA became lower than that of the as-deposited Si film, due to the change from hopping based conduction to activated conduction. Although a band gap was formed for the Si films after the BLDA below 5 W. By the effect of H_2 annealing at 5 W, the defects density at the grain boundaries and within the crystal grains was not reduced sufficiently. Therefore, a considerable number of carriers generated under light exposure were trapped, and the resulting photocurrent of the Si films after the BLDA below 5 W was lower than that of the as-deposited Si film. Although it is well known that the absorption coefficient of light exposure is higher for a-Si films than for poly-Si films, the conclusion is qualitatively valid.

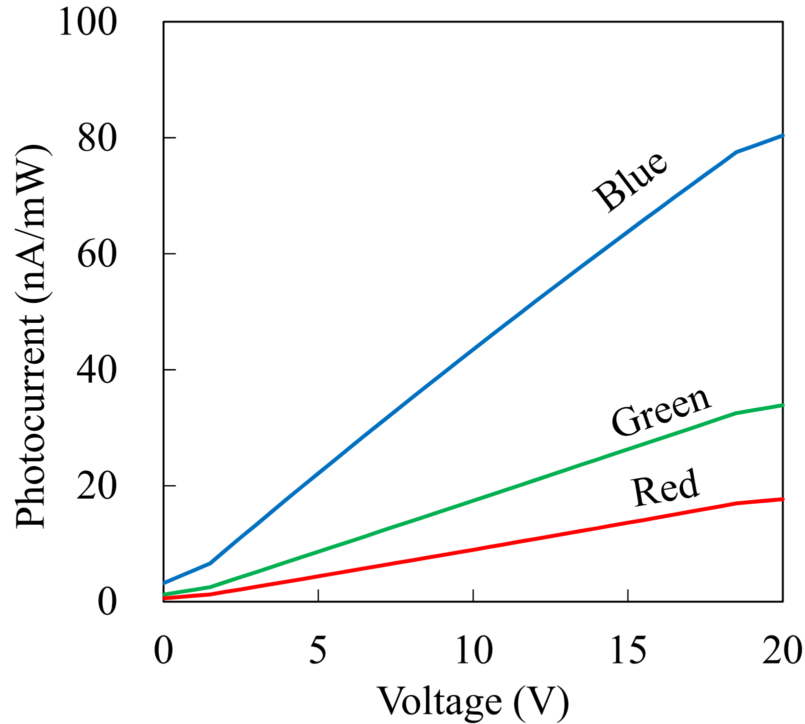

Fig. 2.5 Photocurrents of the Si film after the BLDA at 6 W under red, green, and blue light exposures after normalizing to their values per unit exposure energy (Journal Article [1]).

Figure 2.5 shows the photocurrents of the Si film after the BLDA at 6 W under red, green and blue light exposures. *I*–*V* characteristics were measured under red (41.4 mW/cm^2), green (20.7 mW/cm^2), and blue (26.9 mW/cm^2) light exposures. The photocurrents were normalized to their values per unit exposure energy. Even when the photocurrent increased for the Si film after the BLDA at 6 W, the photocurrent for the red-light exposure was still lower than that for the blue or green light exposure. This is because the absorption efficiencies are different between red, green, and blue light exposures. Further increase in the degree of light absorption for the Si films is required. However, our results suggest that BLDA is promising for photosensor applications in a multifunctional SoP.

2.7 Effect of H_2 Annealing

Figure 2.6(a) shows the dark conductivities of the Si films before and after the H_2 annealing. The dark conductivity slightly increased after the H_2 annealing. It is speculated that this is due to the reduction in the defects density in the Si films. Figure 2.6(b) shows the photoconductivities for the Si films before and after the H_2 annealing. The photoconductivities increased with an increase in the laser power after the H_2 annealing. We think that this is also due to the reduction in the defects density in the Si films. The photoconductivity reached as high as 8.1×10^{-4} S/cm for the Si films after the BLDA at 6 W and after H_2 annealing at 450°C.

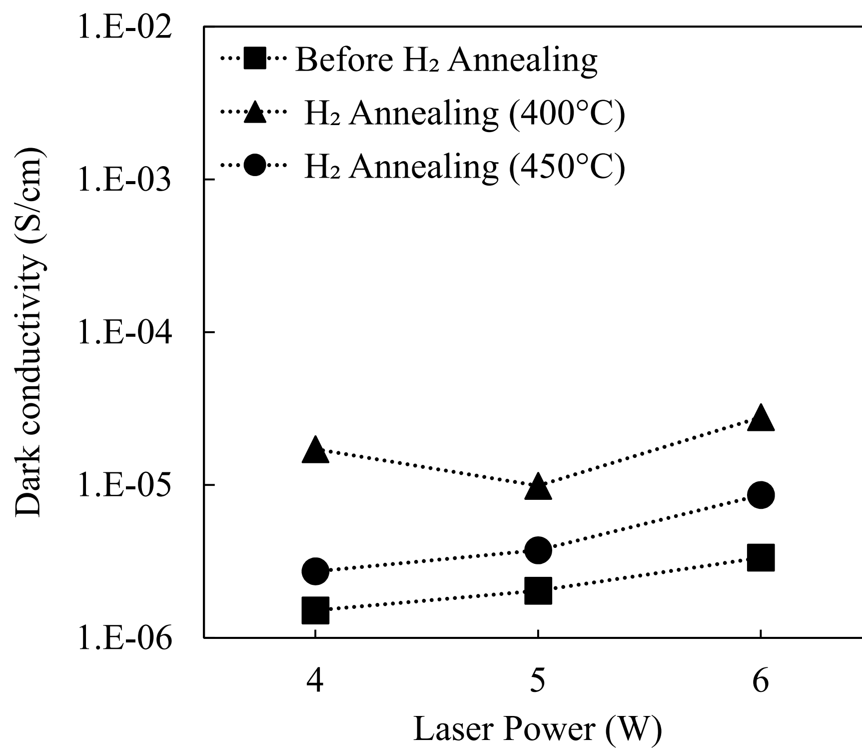

Fig. 2.6 (a) Dark conductivities of the Si films before and after H_2 annealing (Journal Article [1]).

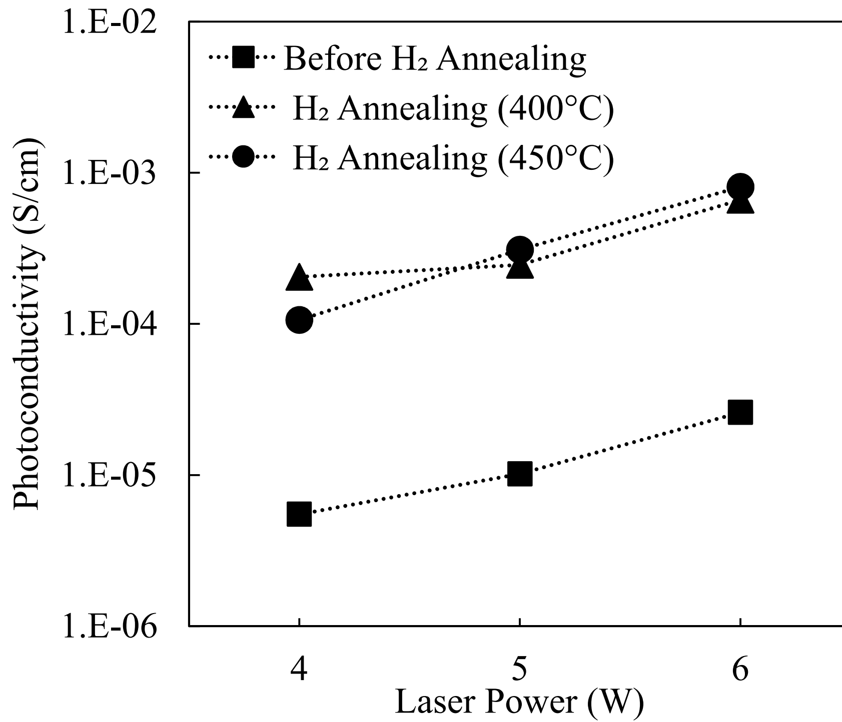

Fig. 2.6 (b) Photoconductivities of the Si films before and after H_2 annealing (Journal Article [1]).

Figure 2.7 shows the photosensitivity ratios ($\sigma_{photo}/\sigma_{dark}$) biased at 20V before and after the BLDA and H_2 annealing. Although a low photosensitivity of 1.7 is seen for the as-deposited Si film, but it slightly improved with increasing laser power. As shown in Fig. 2.1, higher-crystallinity of the Si films are obtained with a higher laser power, and such films showed a higher photosensitivity. Furthermore, a marked improvement in photosensitivity to 93.7 was observed for the Si film after the BLDA at 6 W and after H_2 annealing at 450°C. This high photosensitivity value is obtained as a result of the high crystallinity due to the BLDA at 6 W and the resultant reduction in the defects density in the Si films due to the H_2 annealing at 450°C.

The photoconductivity of Si films after BLDA has been investigated for photosensor applications. Uniform micro grains of approximately 50 nm in diameter were obtained for the Si films after the BLDA at 4 W, and fairly large grains were obtained at 6 W. The photoconductivity of the Si films was improved along with the improvement in their crystallinity when the laser power of the BLDA was increased. After H_2 annealing, the photosensitivity of the films was further improved markedly. High photosensitivity ratio ($\sigma_{photo}/\sigma_{dark}$) of 94 was obtained under white light exposure of 100 mW/cm^2. We suggest the potential of Si films after BLDA for photosensor applications. Because BLDA is a promising technique from the viewpoint

of practical productivity, it is meaningful to integrate simultaneously photosensor devices in the next-generation SoP formed using BLDA.

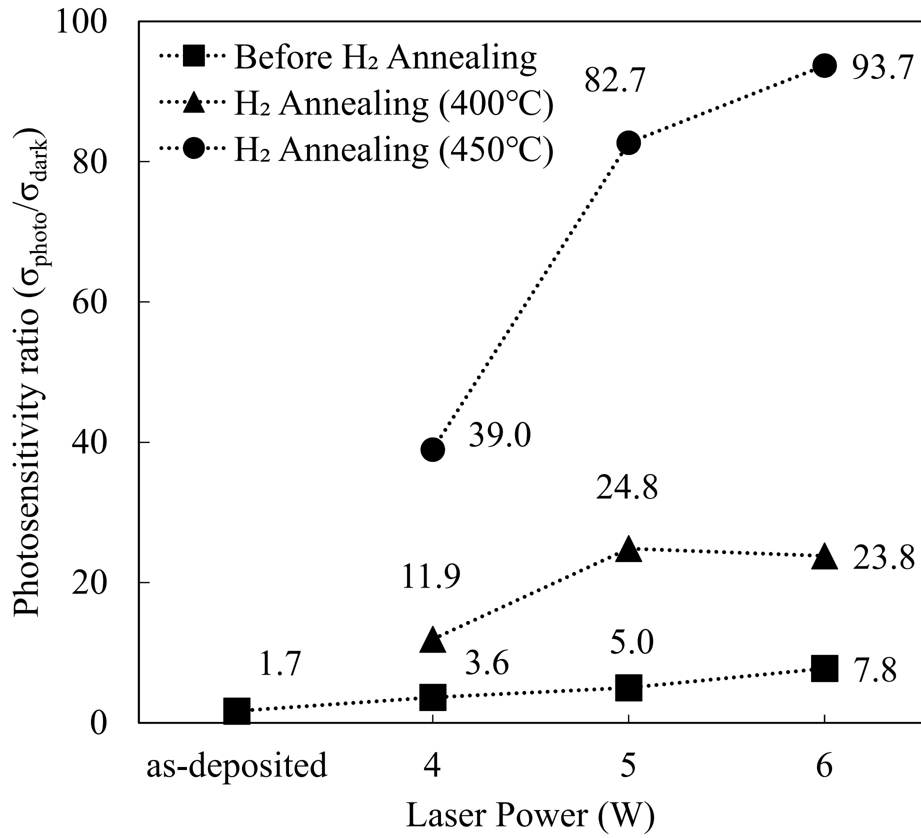

Fig. 2.7 Photosensitivity ratios ($\sigma_{photo}/\sigma_{dark}$) biased at 20 V before and after the BLDA and after H_2 annealing (Journal Article [1]).

References

1) S. Y. Han, K. S. Jeon, M. S. Seo, D. C. Kim, B. Cho, K. Jeong, S. M. Seo, S.-W. Jung, W. Kim, S.-H. Yang, J. Song, H.-S. Kong, and H. G. Kim, SID Symp. Dig. Tech. Pap. **43**, 330 (2012).
2) S. Ahn, S. Jeon, I. Song, Y. Jeon, Y. Kim, C. Kim, J. Lim, W. Jeong, J. Goh, S. Yeon, C. Lee, J. Kim, J. Lee, J. Song, A. Nathan, S. Lee, and U. Chung, SID Symp. Dig. Tech. Pap. **43**, 334 (2012).
3) W.-J. Chiang, C.-P. Kung, S.-W. Chen, C.-C. Chang, and C.-W. Wu, SID Symp. Dig. Tech. Pap. 43, 338 (2012).
4) S. Koide, S. Fujita, T. Ito, S. Fujikawa, and T. Matsumoto, Proc. IDW'06, p. 689 (2006).
5) M. Yamaguchi, Y. Kaneko, and K. Tsutsui, Jpn. J. Appl. Phys. **32**, 458 (1993).
6) H. Miyake, K. Sakai, T. Abe, Y. Sakai, H. Hotta, H. Ito, and T. Ozawa, Jpn. J. Appl. Phys. **29**, L2373 (1990).
7) T. Yamashita, T. Shima, Y. Nishizaki, M. Kimura, H. Hara, and S. Inoue, Jpn. J. Appl. Phys. **47**, 1924 (2008).
8) R. A. Street, J. Graham, Z. D. Popovic, A. Hor, S. Ready, and J. Ho, J. Non-Cryst. Solids **299**, 1240 (2002).
9) S. Tomiyama, T. Ozawa, H. Ito, and T. Nakamura, J. Non-Cryst. Solids **198**, 1087 (1996).
10) M. Kimura, T. Shima, T. Okuyama, S. Utsunomiya, W. Miyazawa, S. Inoue, and T. Shimoda, Jpn. J. Appl. Phys. **45**, 4419 (2006).
11) K. Kanzaki, Dig. Tech. Pap. AM LCD'01, p. 71 (2001).
12) T. Nishibe and H. Nakamura, J. Soc. Inf. Disp. **15**, 151 (2007).
13) T. Mukae, K. Sugihara, T. Sugihara, K. Shirai, T. Okada, T. Noguchi, and T. Ohachi, Proc. IMID, p. 15 (2012).
14) Y. Ogino, Y. Iida, E. Sahota, M. Terao, Y. Chen, and T. Noguchi, Proc. IMID'09, p. 945 (2009).
15) T. Noguchi, Y. Chen, T. Miyahira, J. de Dieu Mugiraneza, Y. Ogino, Y. Iida, E. Sahota, and M. Terao, Jpn. J. Appl. Phys. **49**, 03CA10 (2010).
16) K. Shirai, J. de Dieu Mugiraneza, T. Suzuki, T. Okada, T. Noguchi, H. Matsushima, T. Hashimoto, Y. Ogino, and E. Sahota, Jpn. J. Appl. Phys. **50**, 021402 (2011).
17) K. Shirai, T. Noguchi, Y. Ogino, and E. Sahota, IEICE Trans. Electron. **E93**, 1499 (2010).
18) K. Shimoda, K. Sugihara, T. Okada, and T. Noguchi, Proc. IMID'13, p. 200 (2013).
19) T. Okada, J. de Dieu Mugiraneza, K. Shirai, T. Suzuki, T. Noguchi, H. Matsushima, T. Hashimoto, Y. Ogino, and E. Sahota, Jpn. J. Appl. Phys. **51**, 03CA02 (2012).
20) T. Noguchi, T. Nishinohara, J. D. Mugiraneza, K. Shirai, T. Okada, and T. Itoh, Proc. SID, p. 1129 (2012).

21) H. Kuriyama, T. Nohda, S. Ishida, T. Kuwahara, S. Noguchi, S. Kiyama, S. Tsuda, and S. Nakano, Jpn. J. Appl. Phys. **32**, 6190 (1993).

22) N. Kawamoto, A. Masuda, N. Matsuo, Y. Seri, T. Nishimori, Y. Kitamon, H. Matsumura, H. Hamada, and T. Miyoshi, Jpn. J. Appl. Phys. **45**, 2726 (2006).

23) D. P. Gosain, J. Westwater, and S. Usui, Ext. Abstr. AMLCD'97, p. 51 (1997).

24) H. R. Philipp and E. A. Taft, Phys. Rev. **120**, 37 (1960).

25) J. R. Chelikowsky and M. L. Cohen, Phys. Rev. B **10**, 5095 (1974).

26) T. Noguchi, H. Hayashi, and T. Ohshima, J. Electrochem. Soc. **134**, 1771 (1987).

27) T. Noguchi, Jpn. J. Appl. Phys. **32**, L1584 (1993).

28) M.-K. Ryu, S.-M. Hwang, T.-H. Kim, K.-B. Kim, and S.-H. Min, Appl. Phys. Lett. **71**, 3063 (1997).

29) A. Nakamura, F. Emoto, E. Fujii, A. Yamamoto, Y. Uemoto, K. Senda, and G. Kano, J. Appl. Phys. **66**, 4248 (1989).

30) T. Okada, J. D. Mugiraneza, K. Shirai, T. Nishinohara, T. Mukae, K. Yagi, and T. Noguchi, Proc. AWAD'12, p. 85 (2012).

Chapter 3

Multilayer Structure for Photosensor Application

3.1. Introduction

In current evolving information society, consumer personal devices such as mobile phones, television sets, laptop computers, tablets etc. have been continued rapid growth. Flat panel displays (FPD) used in these products have a great demand on downsizing, multi-function, lower power consumption and less material usage while developing high resolution, high color quality, high definition, high brightness. FPDs have accomplished an important role in viewing information. After cathode ray tube (CRT) displays, the market has been occupied by active matrix (AM) flat liquid crystal displays (LCD), adopting hydrogenated amorphous Si (a-Si:H) TFTs or low-temperature polycrystalline silicon (LTPS) TFTs [1, 2].

Most of those new displays are integrated with system on glass (SoG) technology [3, 4]. In addition, recently, photosensitive type touch panels are to be used. In this type of touch panels [5, 6], photosensors which detect light can be integrated inside the touch panel pixels [7-9]. The panel recognizes the touched area by detecting the reflected light. Lateral PIN photodiodes can be produced with identical process at the same time as the TFT fabrication process. Thin-film photosensors are expected as an input device in combination with a display panel. Especially in light sensors which can automatically adjust the brightness of displays, touch panels which can detect the position by laser light or by shade and in two-dimensional contact-type image scanners. Researches on thin-film photosensors are not sufficiently evaluated yet.

In this chapter, photoelectric film was fabricated with the proposed multilayer structure [10]. Possibility of crystallization by performing BLDA for the Si film on underlying metal was investigated. After pre-deposition of buffer layer SiO_2 of 50 nm thickness to block the impurities from the glass, Si layer of 50 nm thickness was deposited by RF sputtering using a semi intrinsic Si target (5-10 Ωcm, n-type) at room temperature. Deposition was carried out at RF power of 450 W and Ne was used as the sputtering gas as the Si film is kept fairly high deposition rate. Ne gas of lower mass number is much easily effused out than Ar gas during high temperature heating [11, 12]. Gas pressure and flow rate was controlled at 1.4 mTorr and 13 sccm. The Si films were crystallized using BLDA at 5 W with a beam size of 600 x 2.4 μm^2 at a scanning speed of 500 mm/s. The applied laser power was controlled to 5 W. Samples were annealed in H_2/N_2 (4%) ambient at 450°C for 1h.

To evaluate the crystallinity of Si film, the refractive index (n), the extinction coefficient (k) and the thickness (d) of the Si films were deduced from SE analysis using Sellmeier relationship [13]. To see the

grain structure, Transmission Electron Microscopy (TEM) analysis was done. For both as-deposited a-Si and for subsequently BLDA treated samples, the Si films were patterned with L/W = 5 μm/10 μm for the light absorbed area by photo-lithography. Photocurrent measurement was carried out under white light exposure of 100 mW/cm^2. Photoconductivity of Si films after BLDA has been studied for photosensor applications. Then, calculated simulations with proposed multi-layer structure with back-reflection layer were conducted using (Winelli) simulation software. By adding anti-reflection and back-reflection layers, increasing the substantial amount of light absorbance was expected. Ti was used as the back-reflection metal layer. Then, for the proposed multi-layer structure, Ti or Al as a back-reflection layer metal was deposited on glass substrate using vacuum evaporation. As Al with high reflection of low melting metal cannot endure the following BLDA, instead, Ti layer of about 60 nm thickness was deposited using vacuum evaporation, which has transmissivity of less than 10% within 200 to 900 nm wavelength range. Si film of 50 nm thickness was deposited on Ti using same process conditions of the above Si film. The Si films were crystallized using BLDA at 5 W with the same conditions of the above Si film.

Finally, crystallinity of the Si film with Ti back-reflection layer was evaluated by reflectivity measurement using ultraviolet-visible spectrophotometry (UV-Vis). Additionally, the grain structure in the Si film with Ti back-reflection layer was analyzed using X-ray diffraction (XRD).

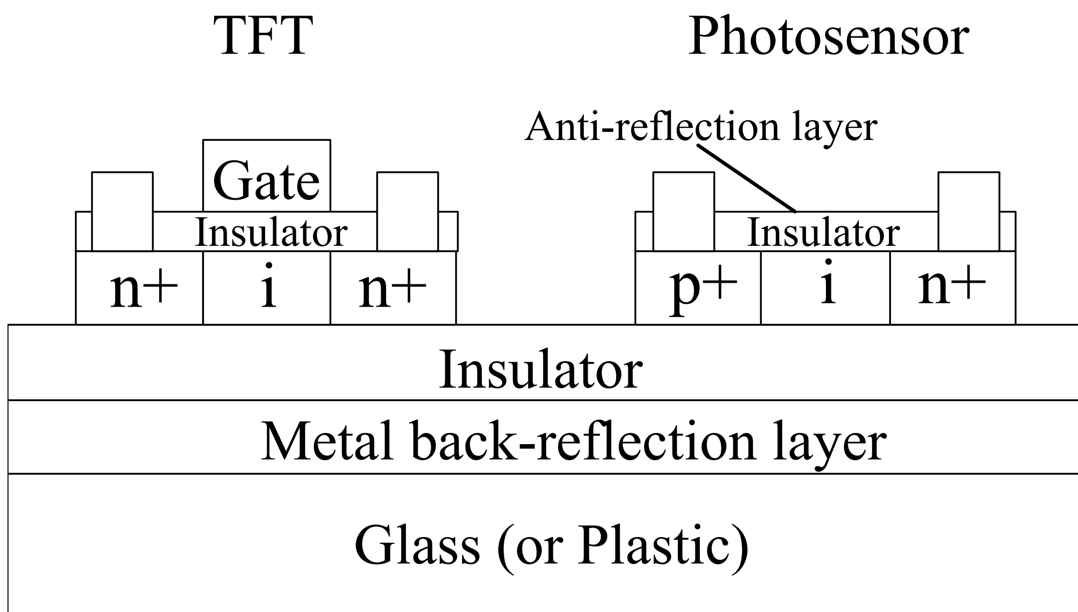

Fig. 3.1 Proposed highly sensitive photosensor structure with multi-layer structure as a TFT system [10].

3.2. Photoelectric characteristics

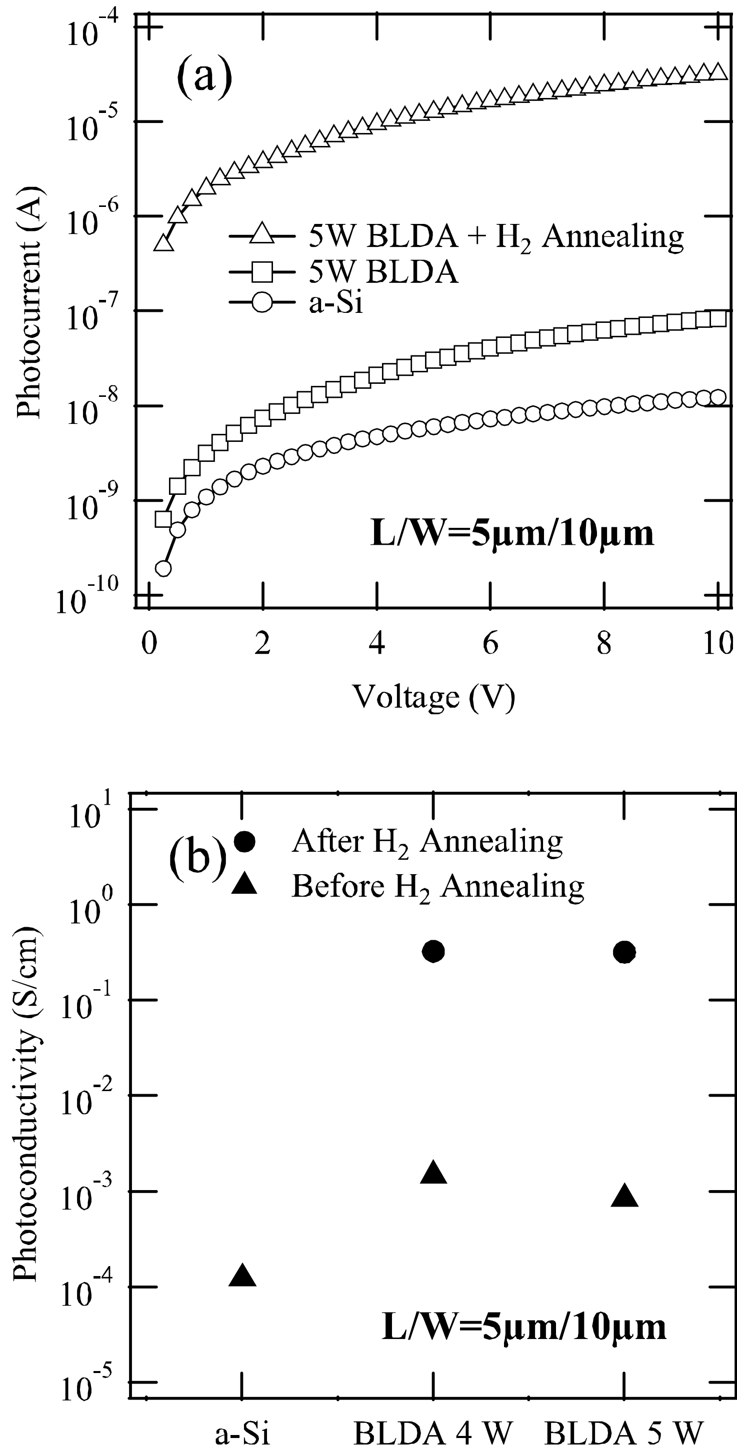

Fig. 3.2 (a) Photocurrent and (b) photoconductive characteristics before and after H_2 annealing under white light exposure of 100 mW/cm^2 (Journal Article [2]).

Fig. 3.2(a) shows the results of photocurrent measurement for Si film before and after BLDA at 5 W and after subsequent H_2 annealing. By comparing with dark current level of the a-Si film (1.2 x 10^{-4} S/cm), high photoconductivity of 8.4 x 10^{-4} S/cm was obtained after BLDA (under the bias at 10 V). For the sample after BLDA at 5 W, as a result of H_2/N_2 annealing at 450°C for 1h, photoconductivity increased significantly to 3.1 x 10^{-1} S/cm. It is considered that the carrier mobility (μ) and lifetime (τ) of carriers in the Si films were improved after BLDA. Recombination of carriers by drift current in the light absorbed area was reduced due to the shortening of channel (below 100 μm) after patterning, which is considered to affect the increase in photosensitivity, in spite of the decrease in absorbed total photon number. Fig. 4 shows the results of photocurrent measurement for the Si film under various light exposures. The light of longer wavelength in red region passes through the Si film because crystallized thin Si film cannot absorb red efficiently as well as infra-red (IR) light. In order to improve photosensitivity for red light or infra-red region, a new multi-layer structure had been proposed considering the reflection [10]. Furthermore, additional H_2 annealing is expected to improve further the photosensitivity by terminating the dangling bonds existing at the grain boundaries or the small defects in Si film.

3.3 Simulation Results

By adding anti-reflection or/and back-reflection layers, light absorption can be enhanced. To improve the low photosensitivity, effective multi-layer structure had been proposed (Fig. 3.1). The insulating film formed on the top of lateral photo-sensor layer acts as an anti-reflective layer as well as a gate insulating film for TFT. High quality gate insulator was reported by adopting RF sputtering and was demonstrated in TFTs [14, 15]. By using this proposed structure, substantial light absorbance can be increased selectively in red or in infra-red by the light interference effect. Calculated simulations were performed on the proposed structure using the *n, k* spectra data obtained from the Si film after BLDA at 5 W. The thicknesses of anti-reflection and bottom insulator layers were optimized according to the *n, k* spectra data of Si film after BLDA at 5 W. Winelli in spectroscopic ellipsometry system supported by SOPRA Corporation was used as the simulation software. Fig. 3.3 shows the simulation results of light absorption by adding the multiple layers. Light absorbance was calculated using equation 1.

$$\%A = 1 - (\%R + \%T) \qquad (1)$$

Significant increase in red and in IR light absorption is expected by adjusting and optimizing the interference effect with the proposed structure. The metal as a back-refection layer limits the light transmission through the Si layer. As a result of above two factors, the number of internal reflections increases, and the photocurrent increases. Significant increase in red and IR light was achieved by the implementation of the proposed multi-layer structure. Light absorbance of the sample reached 86% at the wavelength of 680 nm. The optimized thickness for anti-reflection layer was 158 nm and for bottom insulator layer was 161 nm. Furthermore, additional H_2/N_2 annealing is expected to improve further the photosensitivity by terminating the dangling bonds existing at the Si/SiO_2 interface and/or the grain boundaries in Si film. This multi-layer structure is effective not only for Active-Matrix Liquid Crystal Display (AMLCD) but also for Active-Matrix Organic Light Emitting Diode (AMOLED) panel of top emission type.

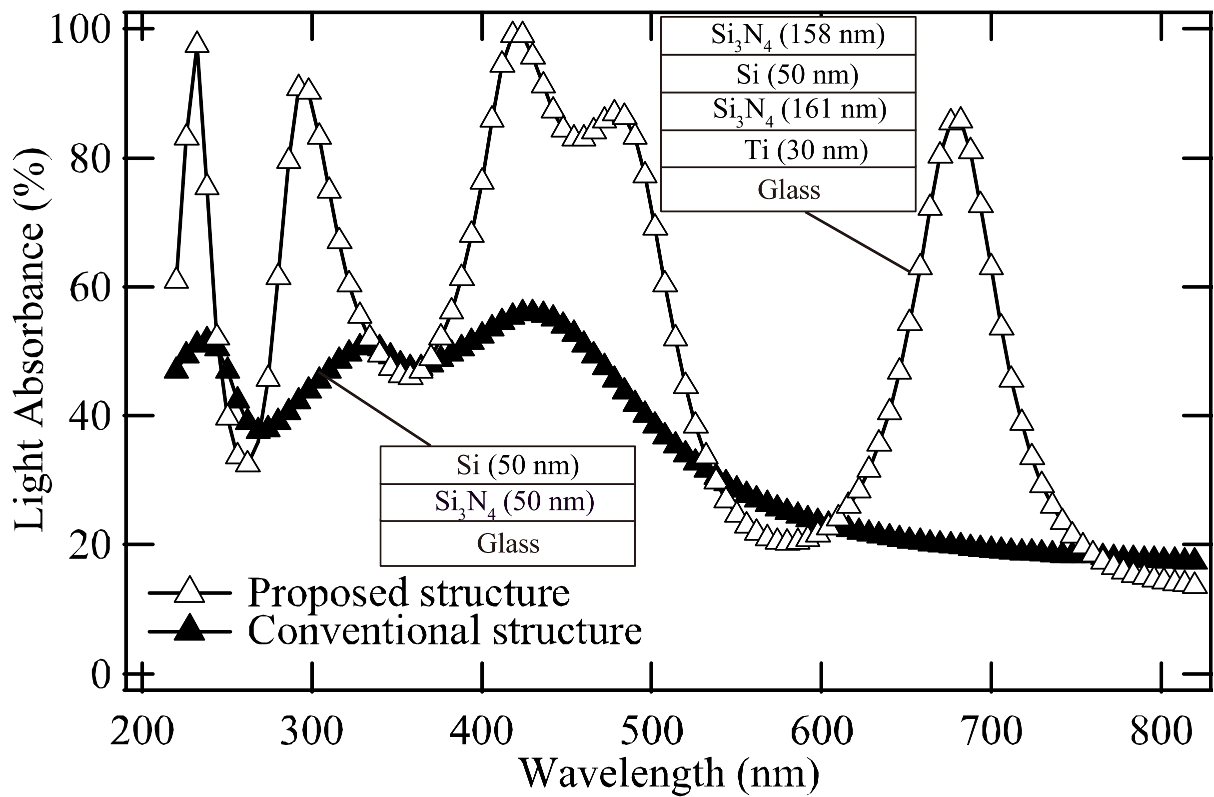

Fig. 3.3 Light absorption rate to the wavelength of multi-layer structure with Ti back-reflection layer (Journal Article [2]).

3.4 Reflectivity Analysis of Multilayer Structure

Total reflectance for both single layer and multi-layer structure with Ti back-reflection layer was measured. Figure 3.4 shows the reflectivity analysis obtained by the Si films before and after the BLDA.

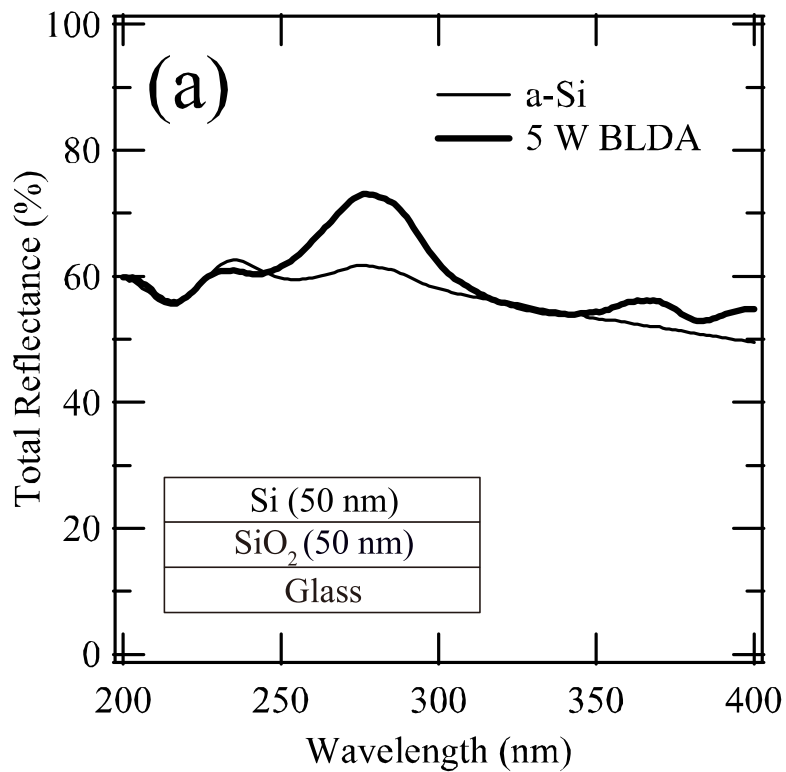

Fig. 3.4 (a) Reflectivity analysis results of single layer (Journal Article [2]).

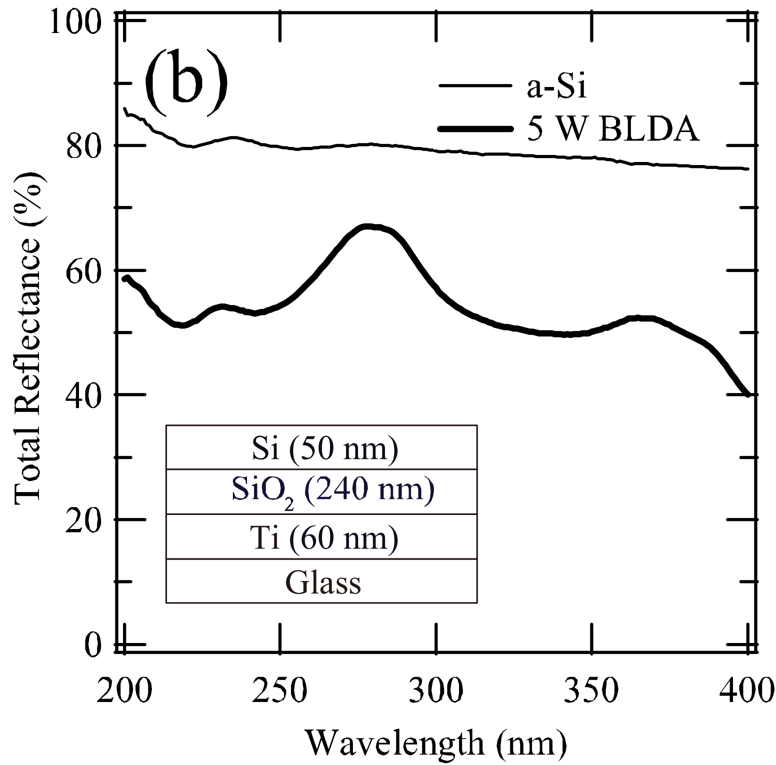

Fig. 3.4 (b) Reflectivity analysis results of multi-layer structure with Ti back-reflection layer (Journal Article [2]).

For the as-deposited a-Si film no peak was confirmed. On the other hand, after performing the BLDA at 4 W, the peak at a wavelength of approximately 280 nm sharpened, and a small shoulder at approximately 360 nm was newly observed. With an increase in laser power to 6 W, the peak became higher, and the shoulder became clearer. For the single-crystal Si, distinct clear peaks were observed at the wavelength. Here, the peaks at approximately 280 and 360 nm correspond to the absorption peaks for the band-to-band transitions of electrons in crystal Si as discussed for Fig. 2.1. Thus, the crystallinity of the Si films can be evaluated from the sharpness of the peaks in the waveform. Therefore, these results indicate that the Si films has become poly-crystalline phase.

3.5 XRD Analysis of Multilayer Structure

Grain structure of the Si film with Ti back-reflection layer on glass was analyzed by X-ray diffraction (XRD). From the results by XRD analysis results as shown in Fig. 3.5, peak of (111) preferred crystal orientation was observed in the vicinity of 28°. Moreover, since the peak is also confirmed in (110) and (311) angles, Si film is believed to be poly-crystallized. Peak at around 38° is presumed to be the peak of the underlying metal (Ti) of the back-reflection layer. Therefore, XRD analysis was carried out for directly Ti film on glass structure. Fig. 3.6 shows the results of XRD analysis for the Ti on glass substrate. From Fig. 3.6, it is confirmed that the peak around 38° is due to the poly-crystallized Si film on Ti back-reflection layer [16, 17]. These results suggest that even Si film on the metal seated structure can be crystallized effectively by BLDA.

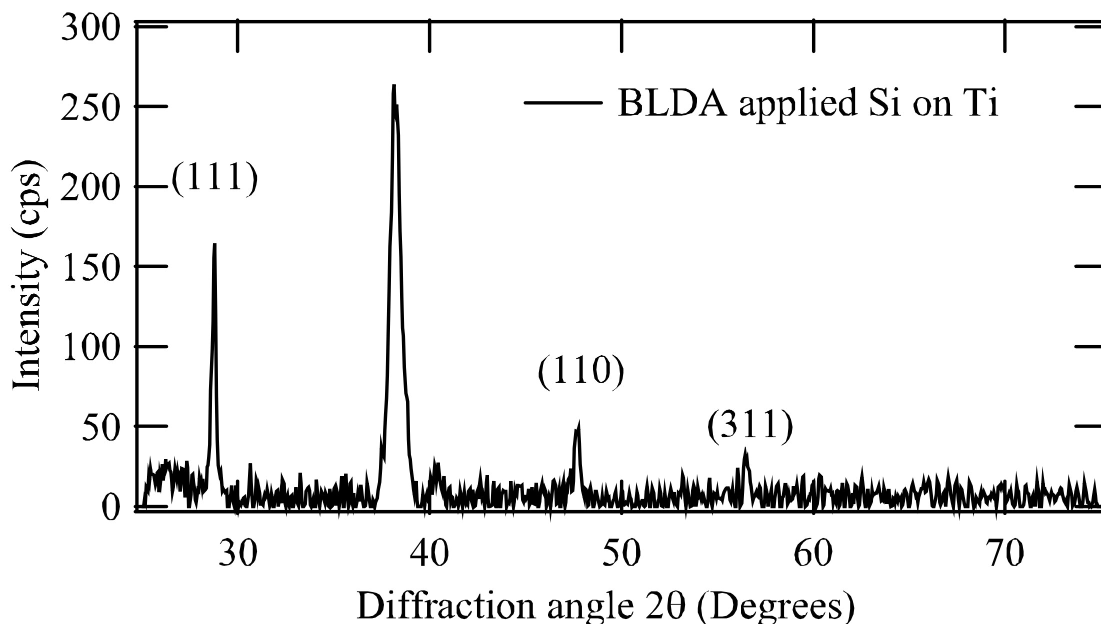

Fig. 3.5 XRD analysis results of Si film with Ti back-reflection layer (1 cm x 1 cm) (Journal Article [2]).

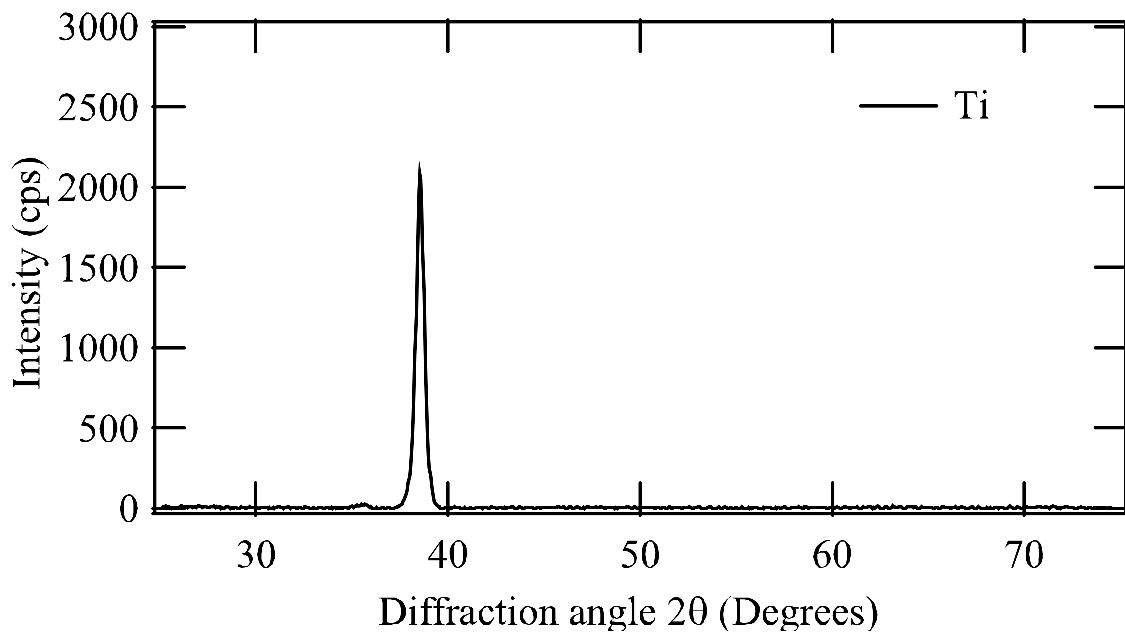

Fig. 3.6 XRD analysis results for Ti layer on glass (2.5 cm x 1.8 cm) (Journal Article [2]).

References

1) C. M. Keum, J. K. Kim, S. J. Moon, S. K. Joo and B. S. Bae, J. of Inf. Disp., vol. **15**, no. 3, pp. 135-138 (2014).
2) N. Matsuo, N. Isoda, A. Heya, S. Amano, S. Miyamoto, T. Mochizuki and N. Kawamoto, Mater. Tran. vol. **51**, no. 8, pp. 1490-1493 (2010).
3) A. Uchikoga, MRS Bulletin, vol. **27**, no. 11, pp. 881-886, (2002).
4) T. Nishibe and H. Nakamura, SID Symposium Dig. Tech. Pap., vol. **37**, no. 1, p. 1091 (2006).
5) M. Yamaguchi, Y. Kaneko and K. Tsutsui, Jpn. J. Appl. Phy., vol. **32**, no. 1, 1, pp. 458-461 (1993).
6) H. Miyake, K. Sakai, T. Abe, Y. Sakai, H. Hotta, H. Ito and T. Ozawa Jpn. J. Appl. Phy., vol. **29**, no. 2, 12, pp. L2373-L2376 (1990).
7) S. Han, K. Jeon, M. Seo, D. Kim, B. Cho, K. Jeong, S. Seo, S. Jung, W. Kim, S. Yang, J. Song, H. Kong, and H. Kim, SID Symposium Dig. Tech. Pap., vol. **43**, no. 1, pp. 330-333 (2012).
8) S. Ahn, S. Jeon, I. Song, Y. Jeon, Y. Kim, C. Kim, J. Lim, W. Jeong, J. Goh, S. Yeon, C. Lee, J. Kim, J. Lee, J. Song, A. Nathan, S. Lee and U. Chung, SID Symposium Dig. Tech. Pap., vol. **43**, no. 1, pp. 334-337 (2012).
9) W. Chiang, C. Kung, S. Chen, C. Chang and C. Wu, SID Symposium Dig. Tech. Pap., vol. **43**, no. 1, pp. 338-341 (2012).
10) T. Mukae, K. Sugihara, T. Sugihara, K. Shirai, T. Okada, T. Noguchi, and T. Ohachi, Proc. of IMID, pp. 15 (2012).
11) T. Noguchi, J. Inf. Disp., vol. **11**, no. 1, pp. 12-16 (2010).
12) T. Noguchi and T. Okada, J. Inf. Disp., vol. **15**, no. 1, pp. 47-51 (2014).
13) G. Jellison, V. Merkulov, A. Puretzky, D. Geohegan, G. Eres, D. Lowndes and J. Caughman, Thin Solid Films, vol. **377-378**, pp. 68-73 (2000).
14) K. Imura, T. Okada, K. Shimoda, K. Sugiharea, T. Noguchi and B. S. Bae, Proc. of IMID, pp. 44 (2014).
15) K. Sugihara, K. Simoda, K. Imura, T. Ashitomi, C. J. Koswaththage, T. Okada and T. Noguchi, Proc. of AWAD, 3A-3, pp.122 (2014)
16) K. Kondoh, T. Threrujirapapong, H. Imai, J. Umeda and B. Fugetsu, J. Nanomater., vol. **2008**, pp. 1-4 (2008).
17) T. Threrujirapapong, K. Kondoh, H. Imai, J. Umeda and B. Fugetsu, Mater. Tran. vol. **50**, no. 12, pp. 2757-2762 (2009).

Chapter 4

Thermal Evaporated InSb film for Magnetic Sensor

4.1. Introduction

Magnetic sensor uses the phenomenon that electrons in the semiconductor are bent by Lorentz force. Hall element uses the potential difference generated at this moment. Magnetoresistive elements are largely divided into the types depending on the material and direction of the magnetic field, such as Spin Hall magnetoresistance (SMR), Anisotropic magnetoresistace (AMR) and giant magnetoresistance (GMR).

In SMR, Indium Antimonide (InSb) is adopted as a material, and when the magnetic force becomes strong, the output becomes large, and the magnetic flux direction is perpendicular to the magnetosensitive surface. For this reason, SMR is used for identification of magnetic ink of bills and used in ATMs and vending machines. Furthermore, InSb is widely used in magnetic field sensors, thermal imaging cameras and infrared detectors due to its high carrier mobility [1–6]. It has led to the evolution not only in small Hall components used in video cassette recorders (VCR), optical drives but also household electrical appliance and car industry [7]. Furthermore, InSb has high expectation in high resolution radiation detectors [8]. InSb thin films can be fabricated with many preparation methods [9–12] Generally, InSb layer with high carrier mobility is obtained by epitaxial growth on single-crystal substrate using expensive process such as molecular beam epitaxy (MBE) [13]. On the other hand, fabricating InSb film on glass substrate has high potential from the perspective of low-cost process and functional applications.

Conventionally, in the Hall device fabrication process, InSb film deposited on mica substrate is thermally annealed to crystallize. Then, the poly-crystallized InSb film is transferred to ferrite substrate. The used mica substrate is discarded. Furthermore, remaining mica on InSb, weak heat resistance of the adhesive between ferrite substrate and the InSb are the issues of this transferring process. Hence, sheet mica is a natural material and its high commercial demand, fabrication on mica substrate is becoming expensive. In this situation, glass substrate is a preferable candidate. In case of forming InSb film on a glass substrate by thermal evaporation, ultra-high mobility TFT circuit equipped with sensitive magnetic element cannot be obtained as the electron mobility is small compared to the case of depositing on conventional mica substrate. Previously, various studies have been done on annealing effect of InSb [14–16]. Enhancing the crystallinity and carrier mobility of thermal evaporated InSb film on glass can be expected by FA, RTA or BLDA [17].

By forming this high-quality film on glass substrate, low-cost, high heat resistance, high productive sensitive magnetic element equipped with TFTs of ultra-high mobility is expected to be realized. In addition,

development of the TFT equipped sensitive magnetic element process on glass and ultra-high-speed Hall IC technology can be expected. In this research, InSb films were deposited on both mica and glass substrates using thermal evaporation and subjected to FA or RTA. Crystallinity, composition and electrical properties of the films were investigated. Pre-annealed InSb films of 1 μm thickness were deposited on glass and on mica substrates using thermal evaporation method. InSb films were annealed using FA or RTA in order to polycrystallize. Sheet resistance of each sample was measured using Four-terminal method. In the range of 200 nm to 900 nm wavelength, spectral reflectance was measured before and after annealing to evaluate the crystallinity of InSb films. Au electrodes were deposited on InSb film using thermal evaporation for electron Hall mobility measurement. Distance among each electrode was 9 mm. Hall effect measurement was conducted under magnetic flux density of 0.31 T and a current of 1 μA.

4.2. Crystallinity evaluation of Furnace Annealed InSb films by TEM

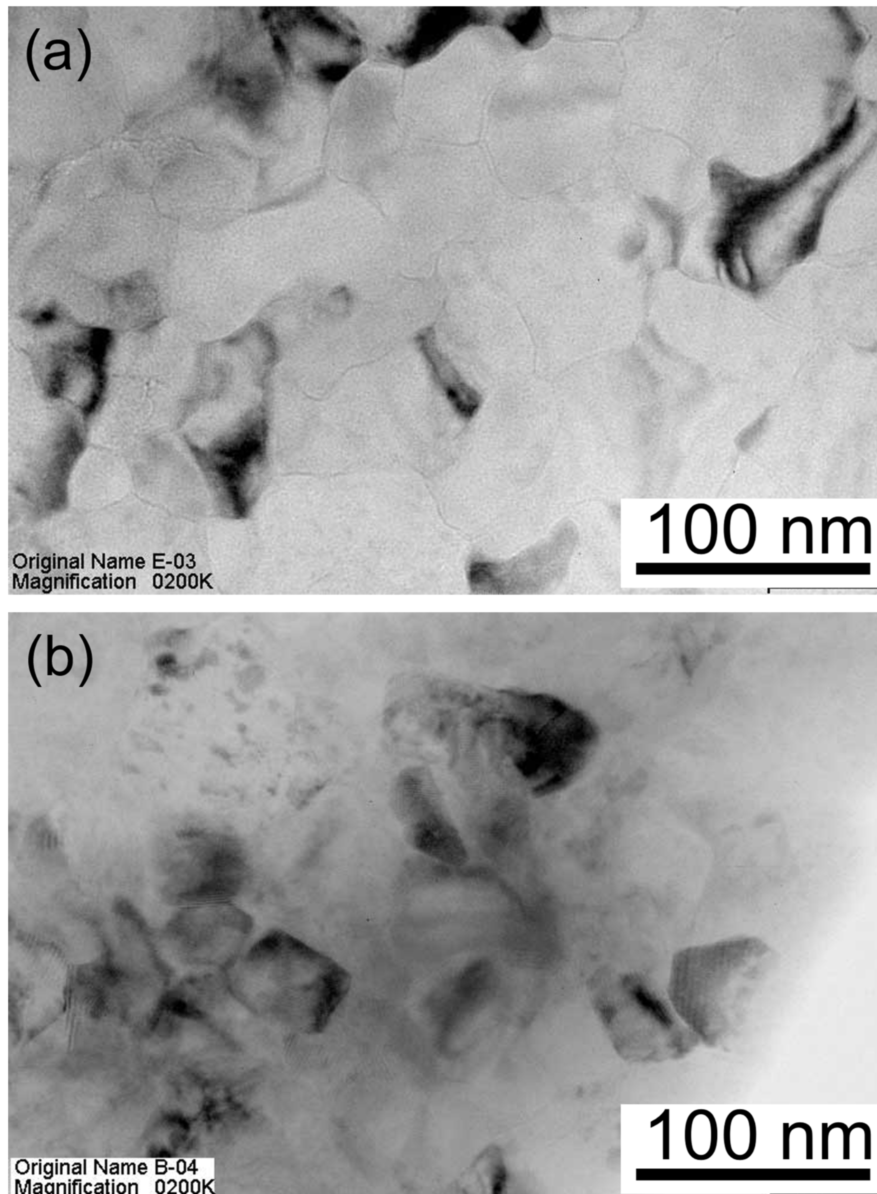

Fig. 4.1 TEM images of the InSb films on (a) mica and (b) glass substrates after FA (Journal Article [3]).

Fig. 4.1 shows TEM images of the InSb films on mica and glass substrates after FA at 500°C for 1 h. As a result of FA, InSb film has been poly-crystallized. Grains ranging from 50 nm to 100 nm in diameter were formed for the InSb film on mica as shown in Fig. 4.1 (a). Compared to InSb on mica substrate, grain size of InSb on glass substrate after FA was not so uniform.

4.3. Crystallinity evaluation of Furnace Annealed InSb films by Spectral Transmittance

Fig. 4.2 shows the optical transmittance results of InSb on mica and on glass after FA for 1 hour. Trend of increasing the optical transmittance was seen with the increase of thermal annealing temperature. Increase in the optical transmission was also seen with the InSb on glass heat-treated at 600°C and InSb on mica heat-treated at 500°C. InSb is not transparent for the wavelengths between 200 nm to 900 nm before annealing. It is considered that optical transmittance of InSb film has been improved due to the increase of crystallinity after annealing. Compared to InSb on glass sample, significant difference of increase in the optical transmittance was observed with InSb on mica substrate. It is speculated that InSb on Mica substrate is crystallized better in quality i.e. higher crystallinity than that of glass substrate.

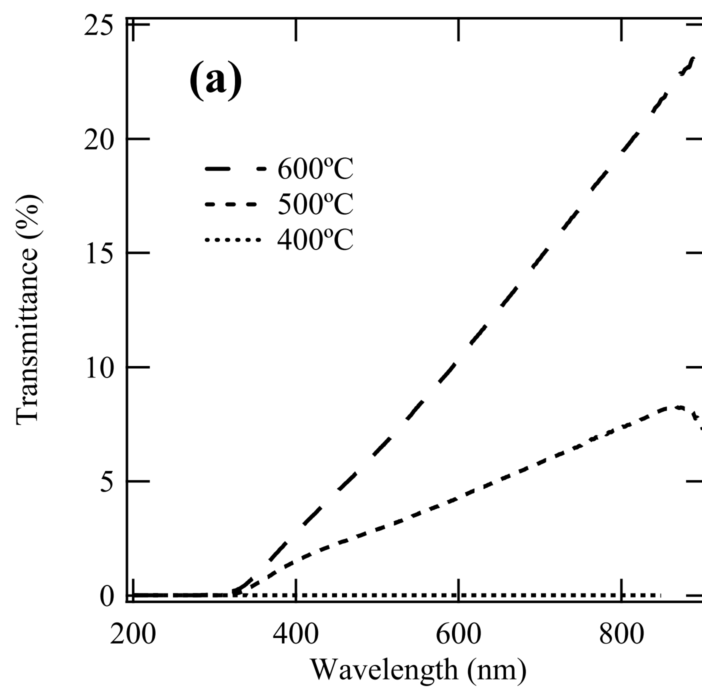

Fig. 4.2 (a) Transmittance of 1 μm thick InSb films on mica substrates after FA (Journal Article [3]).

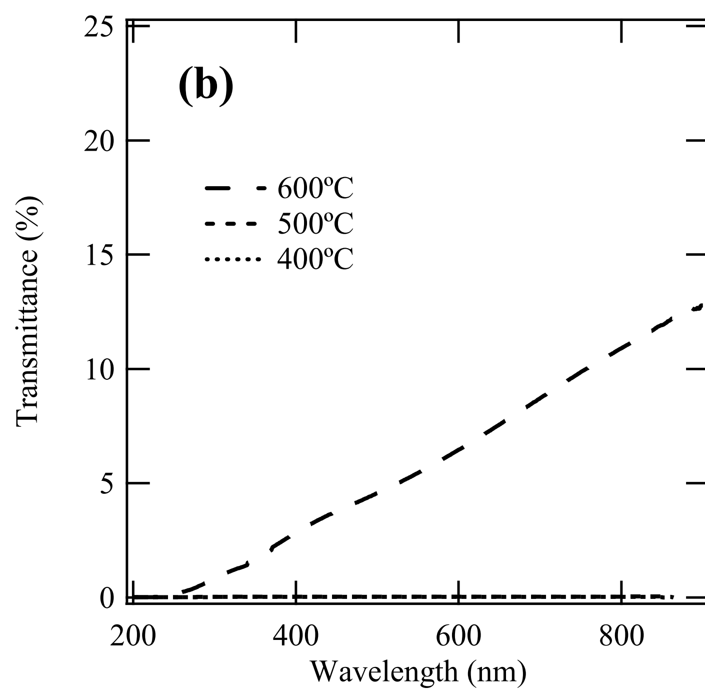

Fig. 4.2 (b) Transmittance of 1 μm thick InSb films on glass substrates after FA (Journal Article [3]).

4.4. Sheet resistance measurement of Furnace Annealed InSb films

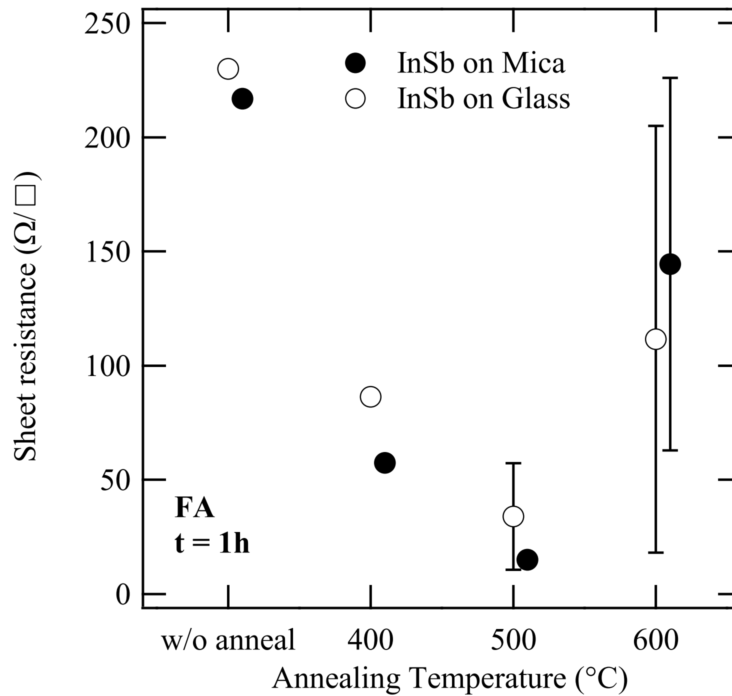

Fig. 4.3 Sheet resistance of InSb before and after FA (Journal Article [3]).

Dependence of the sheet resistance on annealing temperature after FA is shown in Fig. 4.3. The value of sheet resistance was lowest at 500°C for 1 h both on mica and on glass. By increasing the annealing temperature, the variation was observed in the sheet resistance values when it came to 500°C or higher in the case on glass and came to 600°C or higher in the case on mica. Calculated resistivity was as low as 1.06 $\times 10^{-3}$ Ωcm at sheet resistance of 10.6 Ω/□ for the film thickness of 1 μm.

After annealing for 1 h, surface color of InSb films were changed to dark blue. It is speculated that InSb films may have oxidized or film properties may have changed after FA. In Fig. 4.3 it is observed that high temperature annealing after long time (1h~) degraded the film quality. Therefore, RTA was carried out to the thermal evaporated InSb films as described in chapter 4.6. Heated temperature was controlled between 500°C and 540°C.

4.5. Electron Hall mobility measurement for Furnace Annealed InSb films

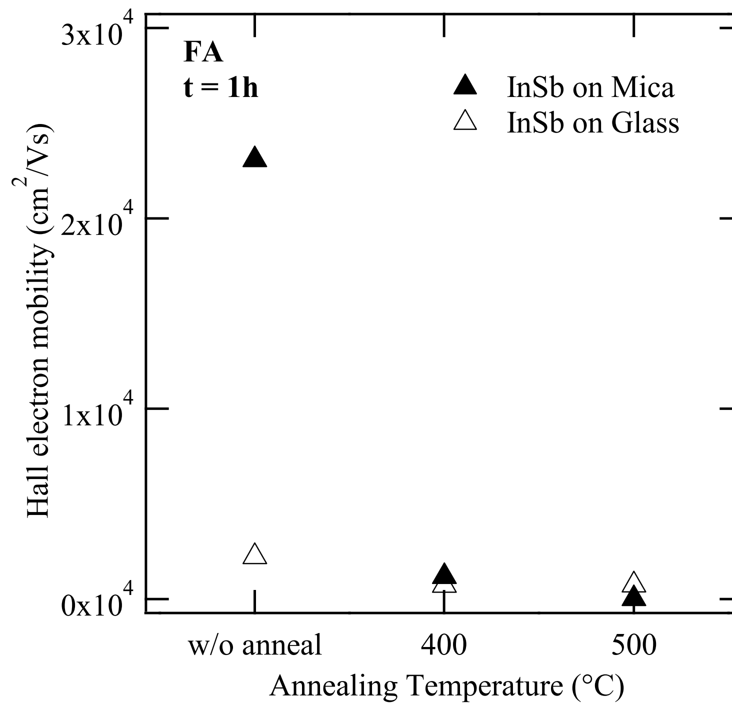

Fig. 4.4 Electron Hall mobility of InSb before and after FA (Journal Article [3]).

Fig. 4.4 shows results of electron Hall mobility for InSb films on both mica and glass substrates before and after FA. 50 nm thick SiO_2 cap was deposited on InSb samples and then, they were annealed at 600°C. Electron Hall mobility of InSb on mica was around 22,000 $cm^2/(Vs)$ and 2,000 $cm^2/(Vs)$ on glass before annealing. However, electron Hall mobility decreased after FA at 400°C for 1 h for the samples on both mica and on glass substrates. Further decrease in electron Hall mobility was observed after increasing the annealing temperature up to 500°C. It is speculated that composition of the InSb (i.e., atomic ratio of In:Sb) has changed after long time annealing. Electron mobility (μ) has decreased due to the change of InSb composition. InSb layer was not remained on the substrate and it shows visibly transparent after annealing at 600°C. As the melting point of InSb is 525°C [18] it is considered that InSb was vaporized at the temperature at 600°C.

4.6. Hall mobility measurement of InSb films annealed by RTA.

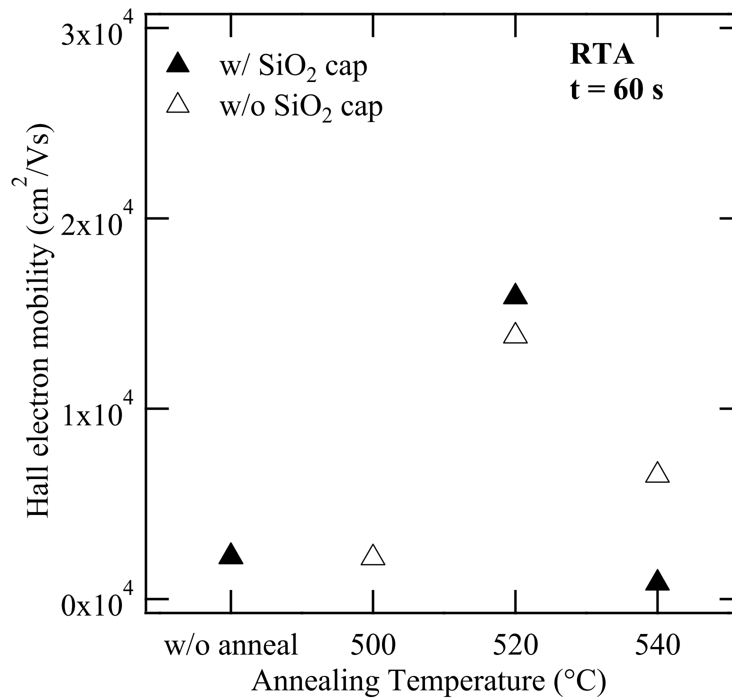

Fig. 4.5 Dependency of Electron Hall mobility on RTA annealing temperature for InSb on glass substrate (Journal Article [3]).

Fig. 4.5 shows the annealing temperature dependency of electron Hall mobility for InSb on glass substrate. Very high electron Hall mobility of about 15,000 $cm^2/(Vs)$ was obtained with the sample annealed at 520°C. As the melting point of InSb is 525°C [18] it is possible that InSb may start to vaporize and the composition has changed at the temperature over 540°C [19]. The highest mobility value was obtained by annealing at 520°C. Annealing time dependency of electron Hall mobility was studied at 520°C from 0 s to 120 s (Fig. 4.6).

4.7. Dependency of Hall mobility on RTA annealing time for InSb on glass substrate.

Annealing time dependency on electron Hall mobility was studied at 520°C from 0 s to 120 s (Fig. 4.6). Average electron Hall mobility of 23,000 $cm^2/(Vs)$ was obtained for the SiO_2 capped InSb films which annealed for more than 30 s. Highest electron Hall mobility around 17,000 $cm^2/(Vs)$ was obtained with the non-capped InSb film annealed for 30 s. However, electron Hall mobility of uncapped InSb films decreased drastically when the annealing time was longer than 30 s. By increasing the annealing time, it is speculated that change of InSb composition or partial elimination by heat may causes the reduction in mobility.

By FA, it is possible to realize large grains when crystallization occurs by applying heat slowly to the InSb film. However, the remained defects concentration seems to be high. By adopting RTA, the generated grain size is smaller than the grains after FA, while the small crystal defects concentration is low. By the crystallization using RTA, it is considered that lifetime and mobility increases mainly due to the reduction of small crystal defects. Effective crystallization with less defects density with keeping the constant composition of In and Sb is speculated as the dominant factor for the high carrier mobility of InSb films after RTA. Therefore, it is considered that the dominant effect is basically the constant composition for the poly-crystalline formation and additional high-quality poly-crystal phase with low defects density should be important.

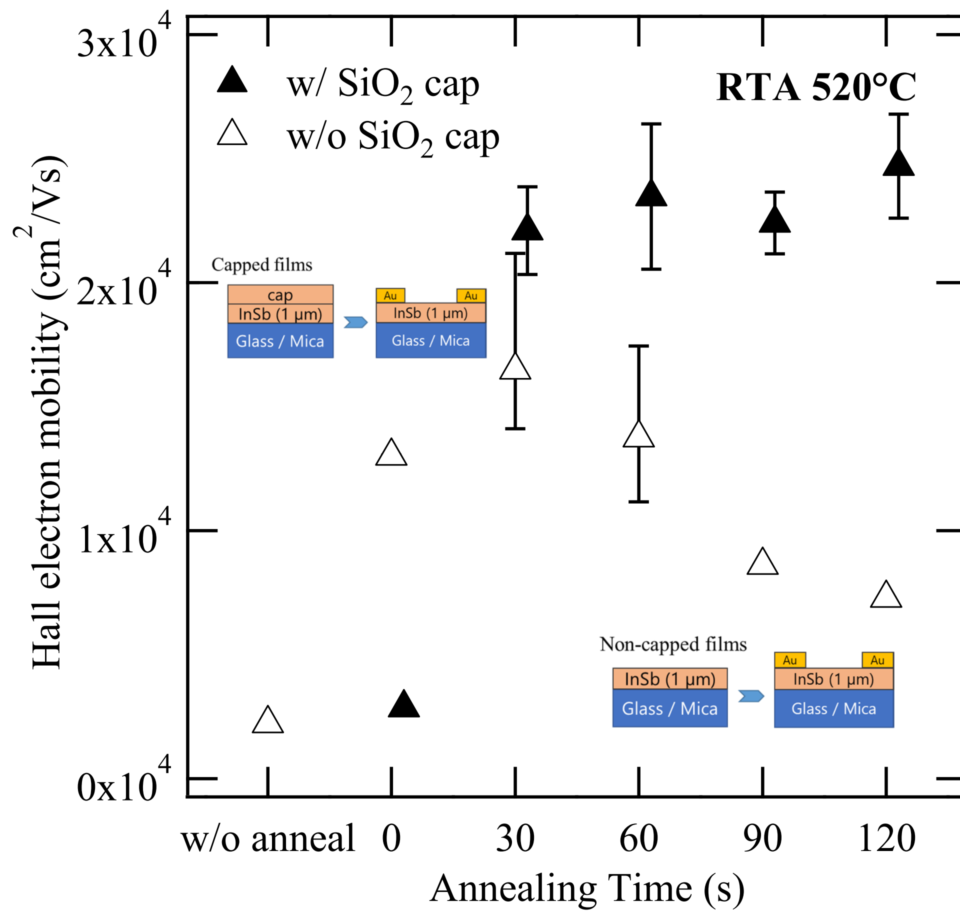

Fig. 4.6 Dependency of Hall mobility on RTA annealing time for InSb on glass substrate. (Journal Article [3]).

4.8. Crystallinity evaluation of Rapid Thermal Annealed InSb films by reflectance spectroscopy.

Fig. 4.8 shows the results of reflectance measurement of 1μm thick InSb films after RTA. Slight peaks around wavelengths of 310, 520 and 660 nm were observed after annealing with capped layer. However, these peaks were hard to be observed, and the reflectivity values were less in the case of uncapped InSb films compared to the capped InSb films. It is speculated that these peaks are correspondent to the extinction coefficient (k) peaks of single crystalline (c-)InSb as in Fig. 4.7 and the appearance of peaks means that the capped InSb films have been crystallized.

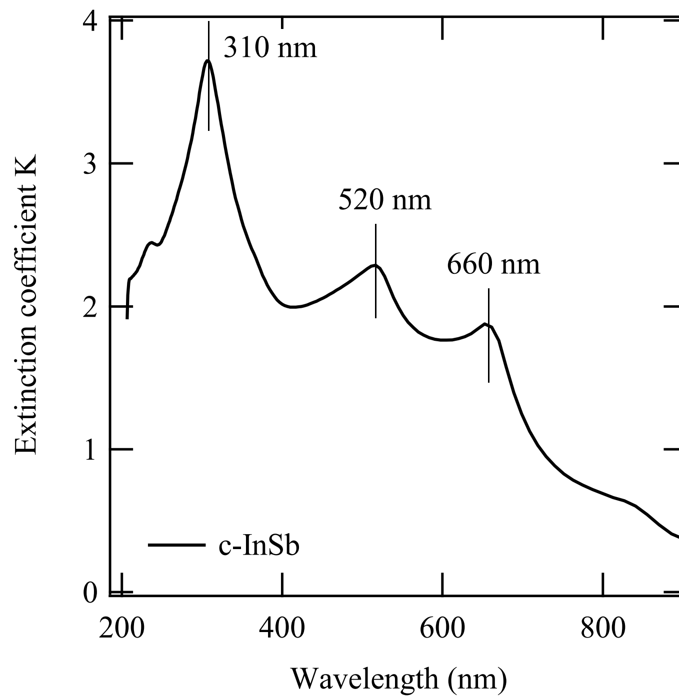

Fig. 4.7 Extinction coefficient of crystalline InSb (Source: Winelli database).

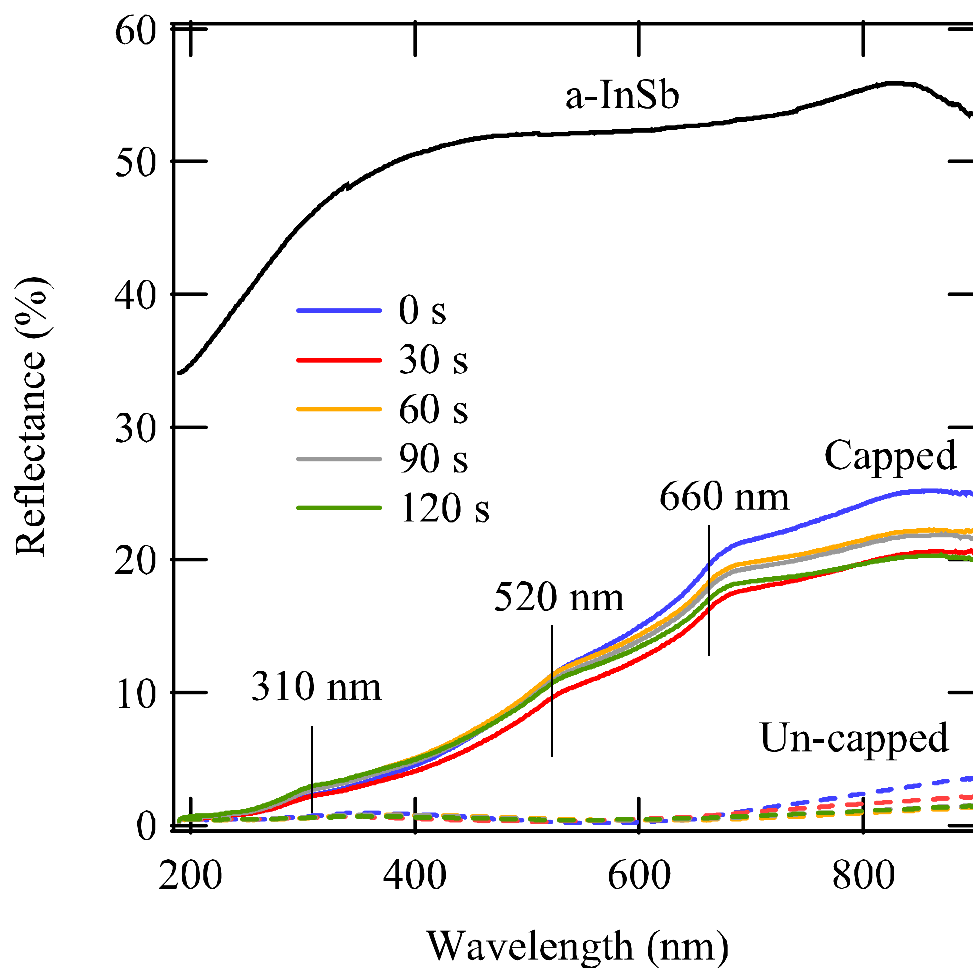

Fig. 4.8 Reflectance of 1 μm thick InSb films after RTA at 520°C (Journal Article [3]).

4.9. In:Sb ratio deduced from Energy-Dispersive X-ray Spectroscopy (EDS)

Table 4.1 EDS analysis of InSb (Journal Article [3]).

	Atomic %				
Annealing time (s)[a]	*In*	*Sb*	*Si*	*O*	*In:Sb*
w/o anneal	48.0	47.3	0.2	4.6	1:1
0	38.0	30.8	2.0	29.2	1:0.8
30	40.7	29.4	0.5	29.5	1:0.7
60	39.9	29.8	0.6	29.7	1:0.7
90	35.1	28.5	0.7	35.7	1:0.8
120	37.9	28.2	0.4	33.6	1:0.7
Annealing time (s)[b]	*In*	*Sb*	*Si*	*O*	*In:Sb*
0	36.2	35.9	4.7	23.2	1:1
30	47.2	44.9	0.6	7.3	1:1.1
60	46.5	44.5	0.9	8.0	1:1
90	45.7	45.5	0.2	8.6	1:1
120	47.3	46.0	1.1	5.6	1:1

[a]w/o SiO_2 cap.
[b]w/ SiO_2 cap.

Table. 4.1 shows the results of energy-dispersive X-ray spectroscopy (EDS) analysis results for both capped and uncapped InSb films before and after RTA. For the uncapped InSb, it appears that the percentage of Sb with respect to In was reduced after annealing. However, ratio of In vs Sb (1:1) is maintained when annealing by keeping the SiO_2 cap. From these results, it is considered that the evaporation of Sb may led the decrease of electron Hall mobility of uncapped InSb films. Studies on temperature dependence of the electron concentration in InSb show that electron concentration increases with the increase in temperature [21]. It is speculated that carrier concentration of InSb increased with the increase of RTA time.

References

31) R. Phelan, Appl. Phys. Lett. **10**, 55 (1967).
32) T. Ashley, A. Dean, C. Elliott, G. Pryce, A. Johnson, and H. Willis, Appl. Phys. Lett. **66**, 481 (1995).
33) I. Bolshakova, Sens. Actuator A-Phys. **76**, 152 (1999).
34) K. Togawa, H. Sanbonsugi, A. Lapicki, M. Abe, H. Handa, and A. Sandhu, IEEE Trans. Magn. 41, 3661 (2005).
35) I. Shibasaki, J. Jpn. Soc. Powder Powder Metall. **61**, S335 (2014).
36) R. Masutomi and T. Okamoto, Appl. Phys. Lett. **106**, 251602 (2015).
37) J. Heremans, D. Partin, C. Thrush, and L. Green, Semicond. Sci. Technol. **8**, S424 (1993).
38) S. H. Park, H. S. Kim, H. S. Shin, H. D. Kim, Y. H. Cho, and Y. K. Kim, J. Korean Phys. Soc. **58**, 1577 (2011).
39) T. Oyabu, SHINKU 19, 304 (1976).
40) S. Song, J. Ketterson, Y. Choi, R. Sudharsanan, and M. Razeghi, Appl. Phys. Lett. **63**, 964 (1993).
41) P. Chiang and S. Bedair, Appl. Phys. Lett. **46**, 383 (1985).
42) S. Y. Han, K. S. Jeon, M. S. Seo, D. C. Kim, B. Cho, K. Jeong, S. M. Seo, S.-W. Jung, W. Kim, S.-H. Yang, J. Song, H.-S. Kong, and H. G. Kim, SID Symp. Dig. Tech. Pap. **43**, 330 (2012).
43) M. Taher, Y. Haga, Y. Nakamura, and O. Nittono, Mater Trans. **46**, 2584 (2005).
44) J. Chyi, D. Biswas, S. Iyer, N. Kumar, H. Morkoc, R. Bean, K. Zanio, H. Lee, and H. Chen, Appl. Phys. Lett. **54**, 1016 (1989).
45) M. Tomisu, N. Inoue, and Y. Yasuoka, Vacuum **47**, 239 (1996).
46) R. Masutomi, M. Hio, T. Mochizuki, and T. Okamoto, Appl. Phys. Lett. **90**, 202104 (2007).
47) E. Dale and G. Senecal, J. Appl. Phys. **33**, 2526 (1962).
48) T. Noguchi, Y. Chen, T. Miyahira, J. de Dieu Mugiraneza, Y. Ogino, Y. Iida, E. Sahota, and M. Terao, Jpn. J. Appl. Phys. **49**, 03CA10 (2010).
49) Y. Hayakawa, Y. Okano, A. Hirata, N. Imaishi, Y. Kumagiri, X. Zhong, X. Xie, B. Yuan, F. Wu, H. Liu, T. Yamaguchi, and M. Kumagawa, J. Crys. Growth **213**, 40 (2000).
50) J. Liu and T. Zhang, Appl. Surf. Sci. **126**, 231 (1998).
51) M. Oszwaldowski and M. Zimpel, J. Phys. Chem. Solids **49**, 1179 (1988).

Chapter 5

Sputtered InSb film for Magnetic Sensor Applications

5.1. Introduction

In chapter 4, high electron Hall mobility of 25,000 cm^2/Vs was obtained with thermal evaporated InSb thin film after RTA. However, in case of mass production, sputtering process has more advantages compared to thermal evaporation. RF sputtering has advantages like high uniformity, reproducibility, low temperature or even room temperature deposition and large area deposition. Therefor low-cost device fabrication can be expected. Furthermore, BLDA is a good candidate for crystallizing InSb film as well as RTA.

In this chapter, crystallinity, electron Hall mobility and surface morphology of annealed InSb film were investigated for magnetic sensor application. Furthermore, effect of various deposition conditions such as gas type (Ne, Ar), gas pressure and film thickness were investigated. Both RTA and BLDA was used to crystallize the InSb films effectively.

First, InSb films of 50 ~ 300 nm thickness were deposited on glass substrate by RF sputtering using an intrinsic InSb target. Deposition was carried out at RF power of 450 W. Ne and Ar gases were used as sputtering gas. Gas pressure was controlled to 1.7 mTorr or 7 mTorr and gas flow rate was controlled to 13 sccm. Then capping layer of 50 nm thick SiO_2 was deposited. For the crystallization by RTA, annealing temperature was controlled between 400 ~ 500°C. In case of BLDA, laser power was controlled to 3 W or 4 W with the beam of 600 × 2.4 μm^2 at a scanning speed of 500 mm/s. Reflectance spectroscopy was used to evaluate the crystallinity of InSb film. Au electrodes were deposited on InSb film using thermal evaporation for Hall carrier mobility measurement.

By forming high quality InSb films on glass and/or flexible substrates, high sensitive magnetic sensor elements equipped with TFTs on system on panel is highly expected.

5.2. Crystallinity evaluation of Rapid Thermal Annealed InSb films by reflectance spectroscopy.

Fig. 5.1 shows reflectance of 300 nm thick sputtered InSb films before and after RTA. Peaks were observed around wavelengths of 310, 520 and 660 nm after annealing with capping layer. It is speculated that these peaks are correspondent to the extinction coefficient (k) peaks of c-InSb as described in Fig. 4.6 and the peaks means that the capped InSb has been crystallized.

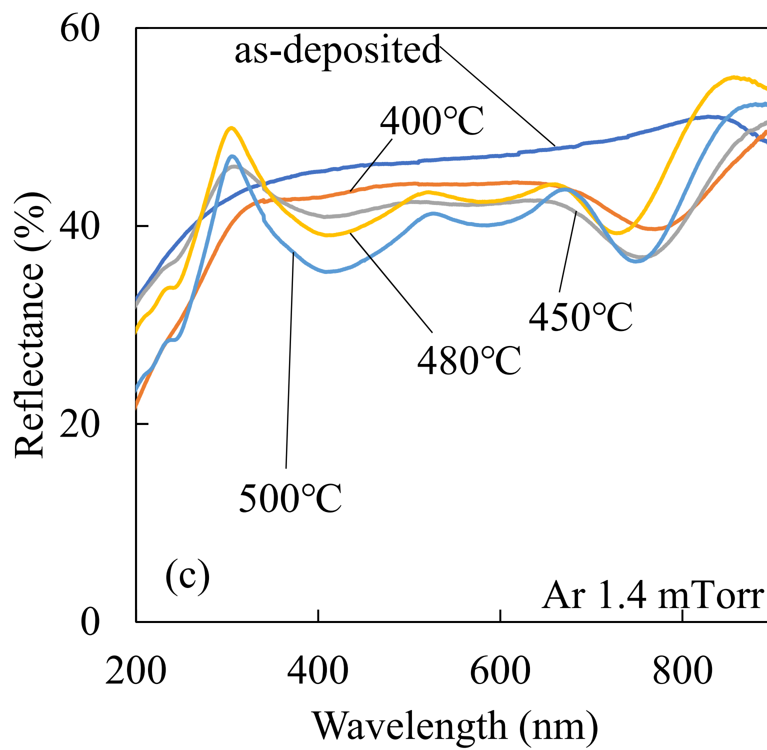

(a) For Ar 1.4 mTorr.

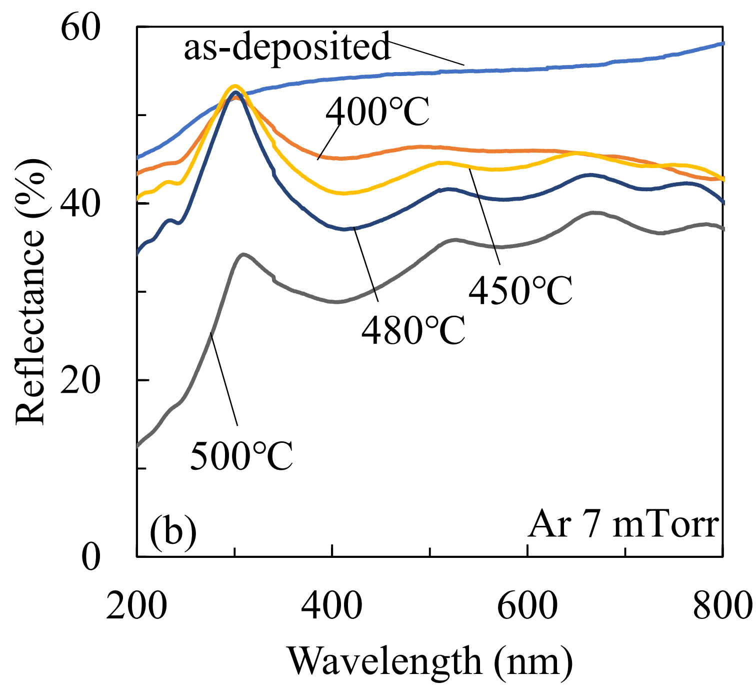

(b) For Ar 7 mTorr.

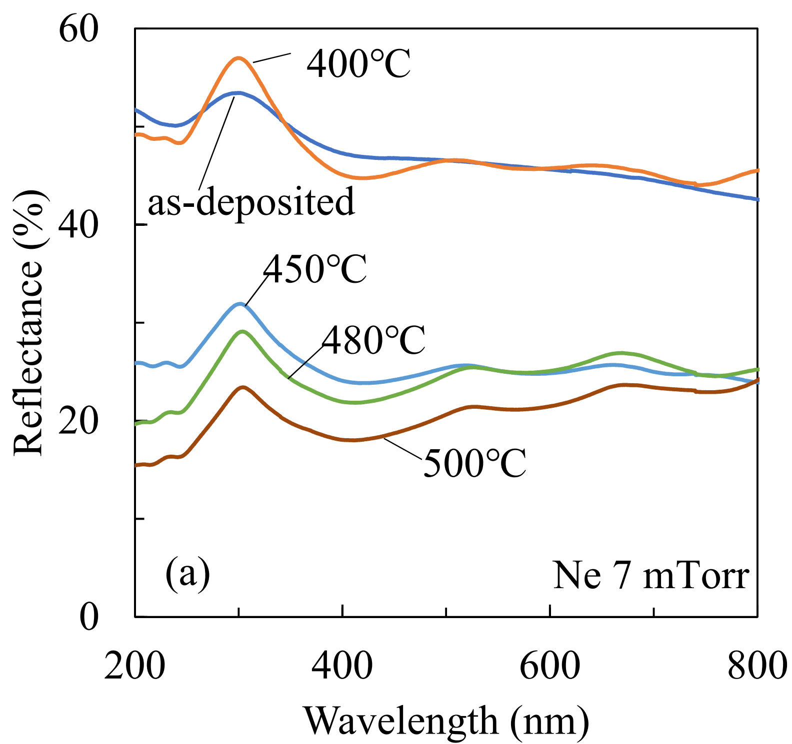

(c) For Ne 7.0 mTorr

Fig. 5.1 Reflectance of 300 nm thick sputtered InSb films after RTA (Conference Article [15]).

5.3. Surface morphology of InSb films after RTA by SEM, AFM

Fig. 5.2 shows the surface morphology of sputtered InSb films before and after RTA. AFM image was taken in a region of 10 × 10 μm^2. The surface roughness increased slightly after RTA. However, the root mean square (RMS) values of the surface was less than 9 nm after applying RTA at 500°C for 30 s.

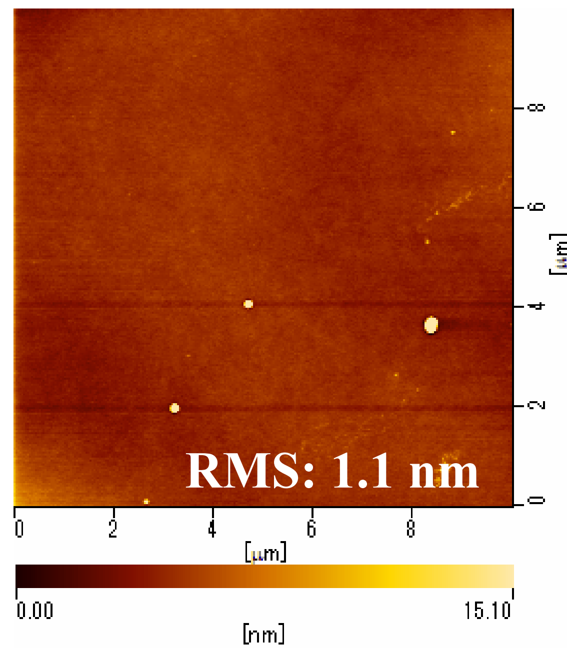

(a) Ar 1.4 mTorr

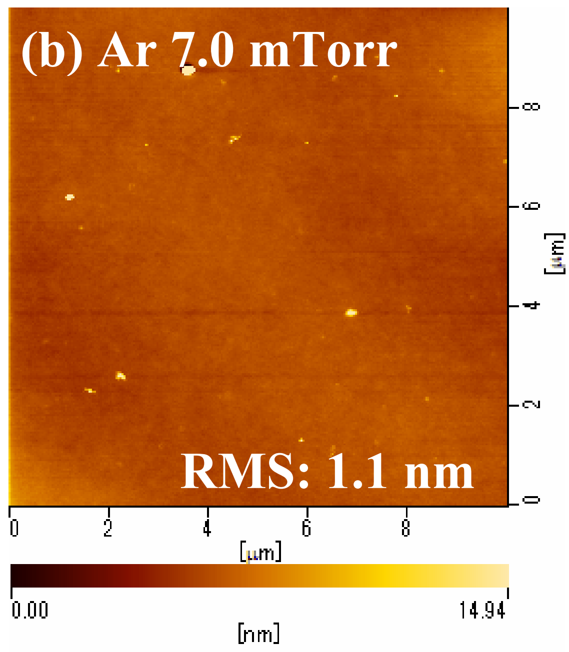

(b) Ar 7.0 mTorr

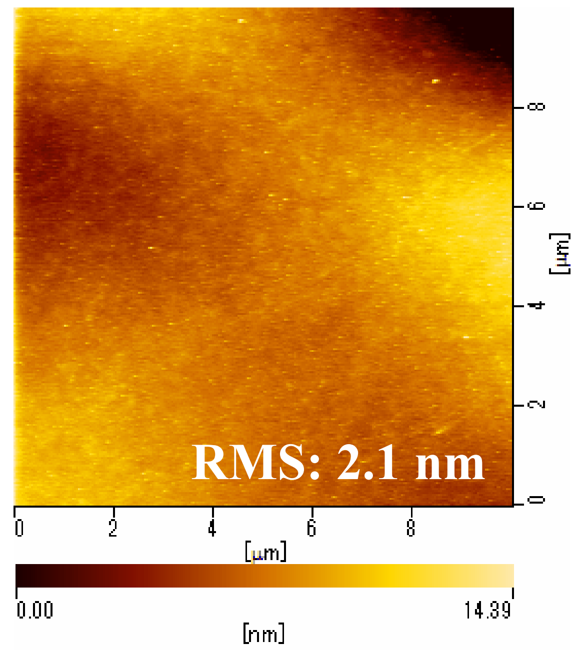

(c) Ne 7.0 mTorr

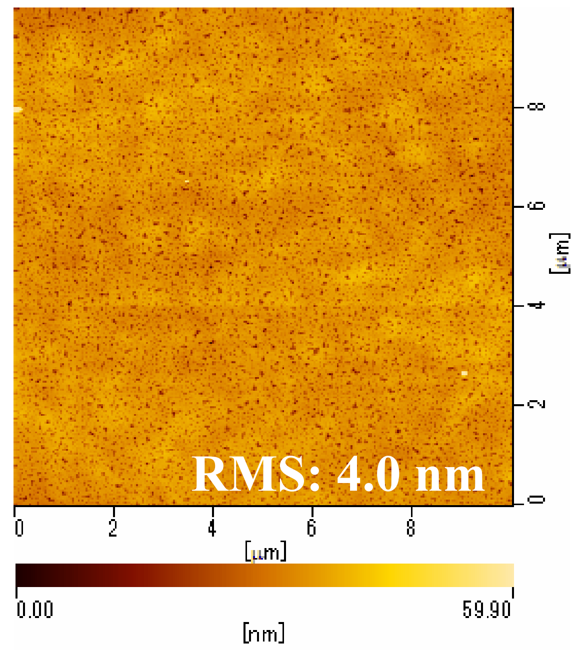

(d) Ar 1.4 mTorr, RTA 500℃ 30s

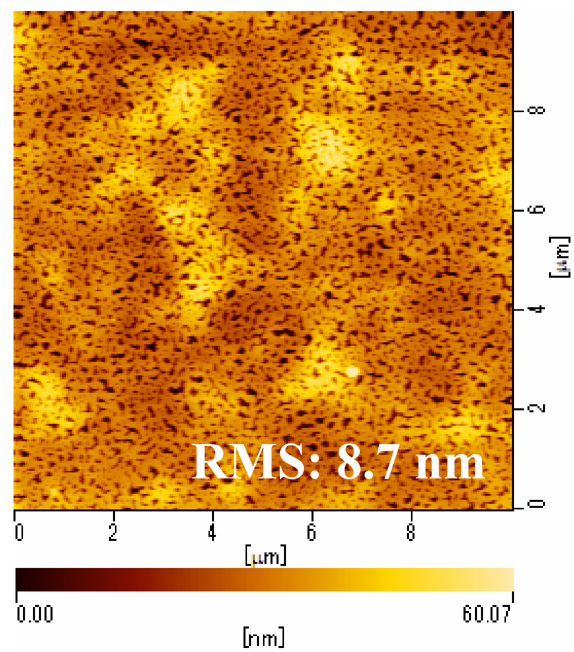

(e) Ar 7.0 mTorr, RTA 500℃ 30s

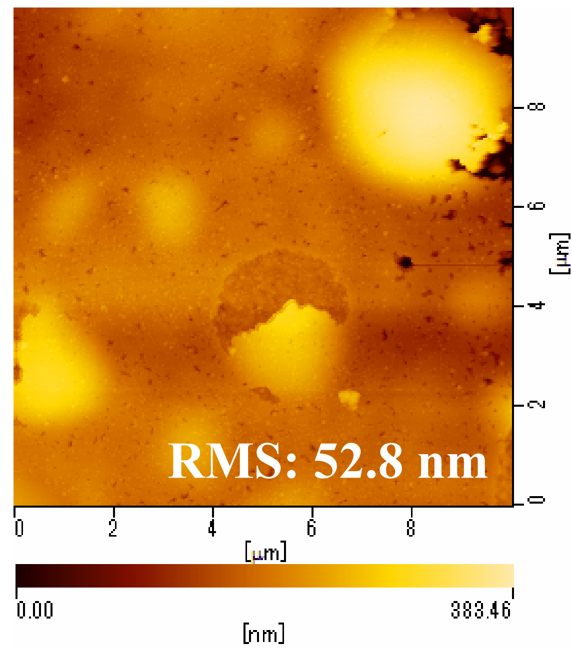

(f) Ne 7.0 mTorr, RTA 500℃ 30s

Fig. 5.2 Surface morphology of sputtered InSb films before and after RTA (Conference Article [14]).

5.4. Electron Hall mobility of InSb films after RTA

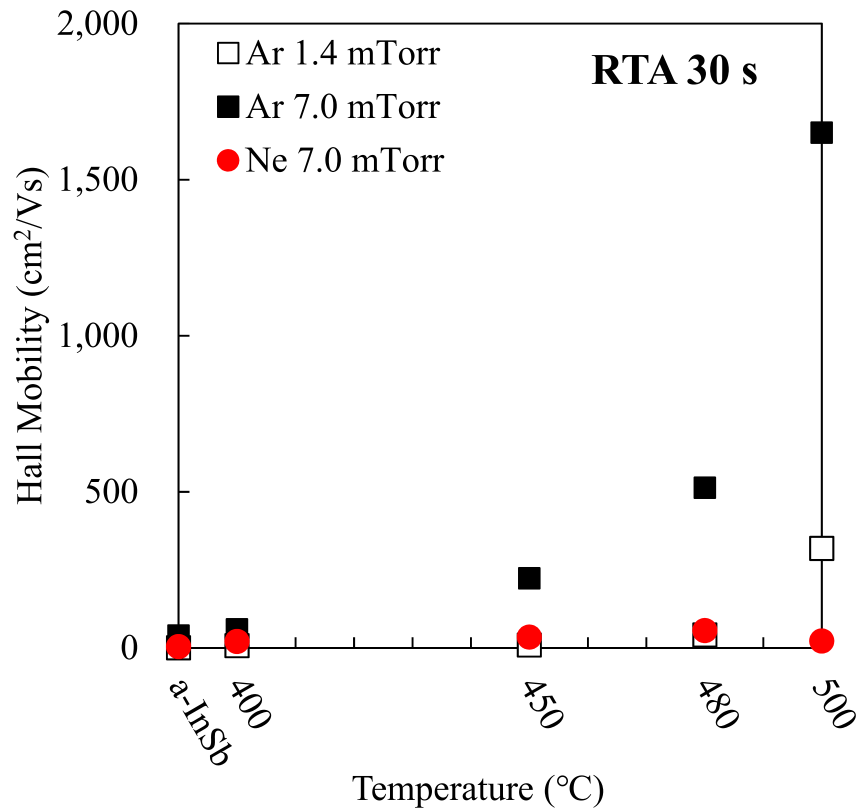

Fig. 5.3 Dependence of electron Hall mobility on RTA temperature (Conference Article [14,15]).

Fig. 5.3 shows the dependence of electron Hall mobility on RTA temperature. Highest electron Hall mobility was obtained with the samples sputtered at 7 mTorr. Furthermore, electron Hall mobility was increased with the RTA temperature and highest electron Hall mobility was obtained at 500°C which is slightly lower than the melting point (525°C) of the single-crystal InSb.

5.5. InSb composition ration by EDS analysis after RTA

Table. 5.1 EDS analysis of InSb films RTA (Conference Article [14]).

		Atomic %		
		In	*Sb*	*In:Sb*
Ne 7 mTorr	as-depo	24.2	22.8	1:1
	400℃	26.6	25.2	1:0.9
	450℃	21.5	22.1	1:1
	480℃	26.6	25.8	1:1
	500℃	21.9	22.2	1:1
Ar 7 mTorr	as-depo	30.3	27.2	1:0.9
	400℃	29.7	26.7	1:0.9
	450℃	31.1	28.1	1:0.9
	480℃	30	27.7	1:0.9
	500℃	28.6	26.3	1:0.9
Ar 1.4 mTorr	as-depo	19.9	17.9	1:0.9
	400℃	15.6	15.1	1:1
	450℃	15.4	14.3	1:0.9
	480℃	14.9	13.5	1:0.9
	500℃	15.2	14	1:0.9

Table. 5.1 shows the energy-dispersive X-ray spectroscopy (EDS) analysis results for InSb films before and after RTA. From the In:Sb composition results, it is certain that ratio of In vs Sb (1:1) is maintained when the films are annealed by keeping the SiO_2 cap. Therefore, SiO_2 capping is effective for RTA.

5.6. Crystallinity evaluation of BLDA applied InSb films by spectral reflectance

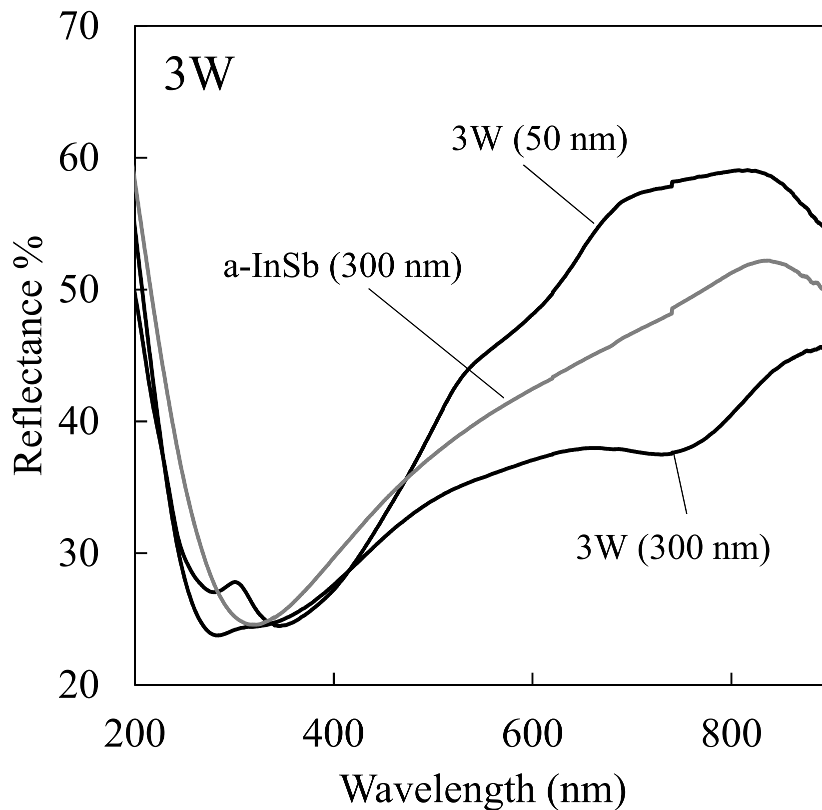

Fig. 5.4 Reflectance of sputtered InSb films before and after BLDA (Conference Article [15]).

Fig. 5.4 shows the reflectance of sputtered InSb films before and after BLDA. Slight peaks were observed around wavelengths of 310, 520 and 660 nm after applying BLDA. It is speculated that these peaks are correspondent to the extinction coefficient (k) peaks of c-InSb as in Fig. 4.6 and the peaks means that the capped InSb has been crystallized.

5.7. Crystallinity evaluation of BLDA applied InSb films by XRD

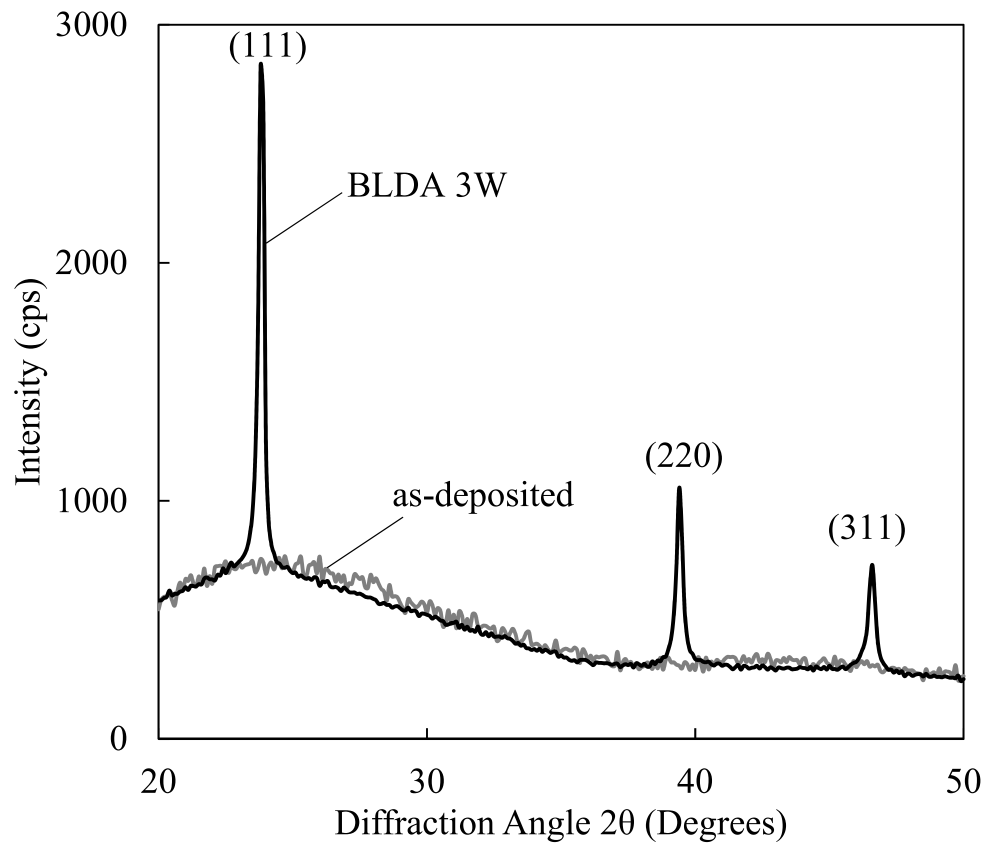

Fig. 5.5 XRD analysis results of InSb film after BLDA (Conference Article [16]).

Grain structure of the InSb film after applying BLDA was analyzed by X-ray diffraction (XRD). From the results by XRD analysis results as shown in Fig. 5.5, peak of (111) preferred crystal orientation was observed in the vicinity of 23°. Moreover, since the peak is also confirmed in (220) and (311) angles, InSb film is believed to be poly-crystallized.

5.8. Surface morphology of InSb films after RTA by SEM

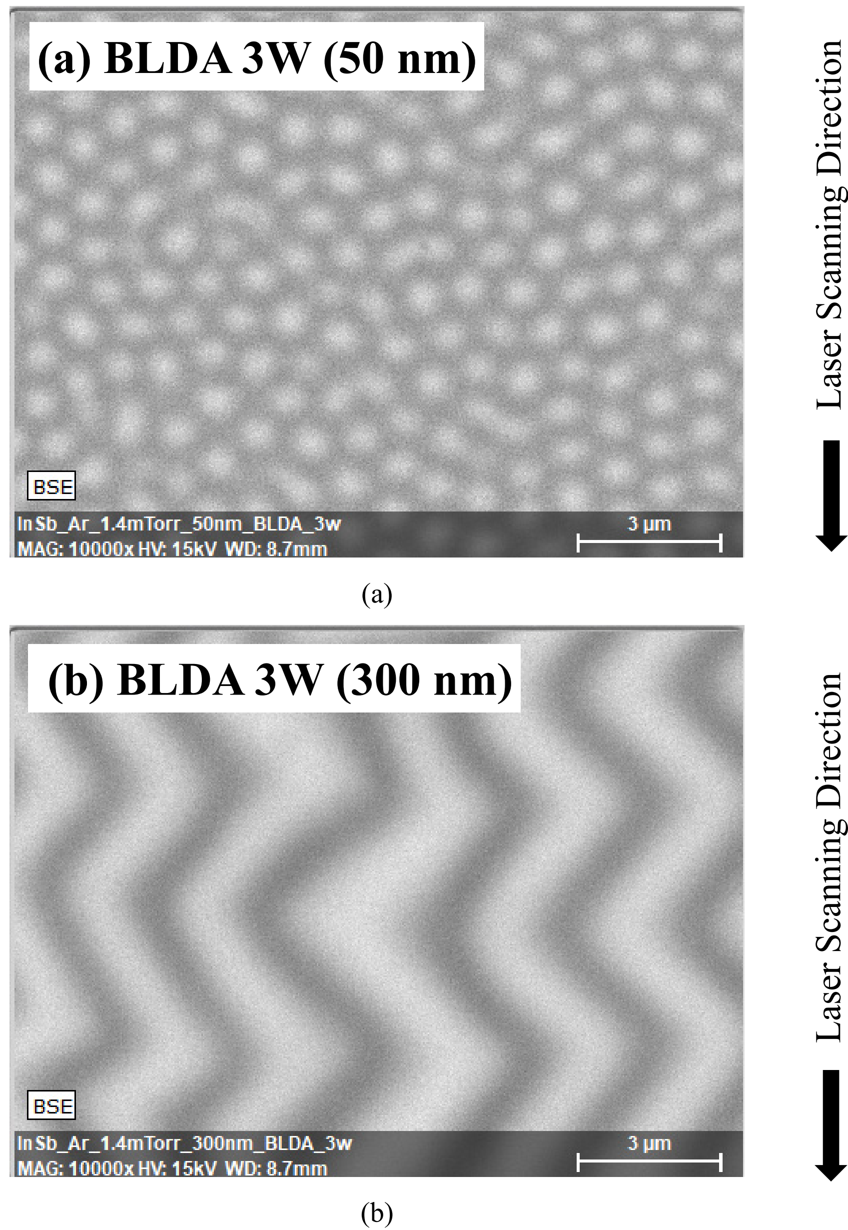

Fig. 5.6 Surface morphology of sputtered InSb films before and after BLDA (Conference Article [15]).

Fig. 5.6 shows the surface morphology of sputtered InSb; (a) for the film of 50 nm thickness after BLDA, (b) for the film of 300 nm thickness after BLDA. Compared to 50 nm thick InSb film, long and continuously large grain-like structure was observed by Scanning electron microscope (SEM) image. It is speculated that large grains are formed with thick films.

5.9. InSb composition ration by EDS analysis

Table. 5.2 EDS analysis of InSb films before and after BLDA (Conference Article [15]).

		Atomic %		
Ar 1.4 mTorr		*In*	*Sb*	*In:Sb*
50 nm	as-depo	19.9	17.9	1:0.9
	3 W	15.1	13.8	1:0.9
	4 W	14.9	13.4	1:0.9
300 nm	as-depo	19.9	17.9	1:0.9
	3 W	14	13.3	1:0.9
	4 W	14.2	13.3	1:0.9

Table. 5.2 shows the energy-dispersive X-ray spectroscopy (EDS) analysis results for InSb films before and after BLDA. From the In:Sb composition results, it is certain that ratio of In vs Sb (1:1) is maintained when the films are annealed by keeping the SiO_2 cap. Therefore, SiO_2 capping is effective not only in RTA but also BLDA.

5.10. Electron Hall mobility of InSb films after BLDA

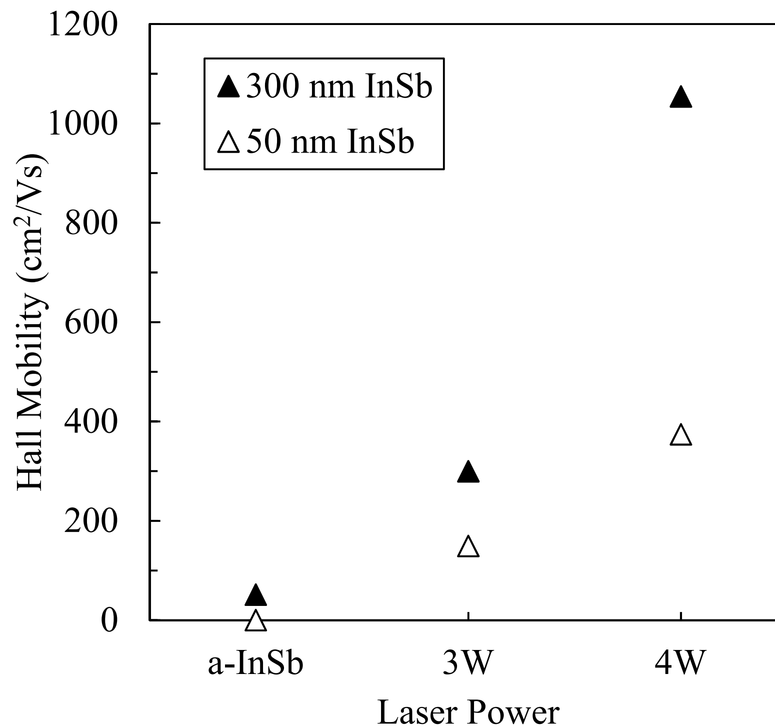

Fig. 5.7 Dependence of electron Hall mobility on laser power (Conference Article [15]).

Fig. 5.7 shows the dependence of electron Hall mobility on laser power for the InSb samples sputtered with Ar gas at a pressure of 1.4 mTorr. Electron Hall mobility was measured for the samples of both 50 nm and 300 nm thickness. High electron Hall mobility was obtained with InSb films of thicker 300 nm film than that of 50 nm thick film. In case of changing BLDA power, higher electron Hall mobility was obtained for the film with rather higher 4 W laser irradiated sample than that 3 W laser irradiated film. It is speculated that large grains are expected to be formed with thicker films at high laser power condition.

5.11 De-gas analysis of InSb films

De-gas analysis of InSb films were conducted using Temperature Desorption Spectrometry (TDS). InSb film of 300 nm thickness was deposited using RF sputtering at the pressure of 7 mTorr. For the InSb film deposition, Ar was used as the sputter gas. After InSb deposition, one of the sputtered film was capped with 50 nm thick SiO_2 film by sputtering. Furthermore, per-annealed thermal evaporated InSb film of 1μm thickness and SiO_2 was also prepared. All films were subjected to TDS (Device name: ESCO TDS 1200 II). Temperature was increased from room temperature to 600°C at the rate of 60°C/min in a vacuum of $1\times10^{-7} \sim 1\times10^{-8}$ Pa.

Fig. 5.8 shows the TDS results of InSb film for (a) O, (b) Ne and (c) Ar gasses. For sputtered film, gas release started early (490°C) in the case of non-capped film than that of capped film (510°C). This proves that SiO_2 capping is effective. Any of the gas was not released for the non-capped thermal evaporated InSb film. This suggests that evaporated InSb film has less impurities than that of sputtered film.

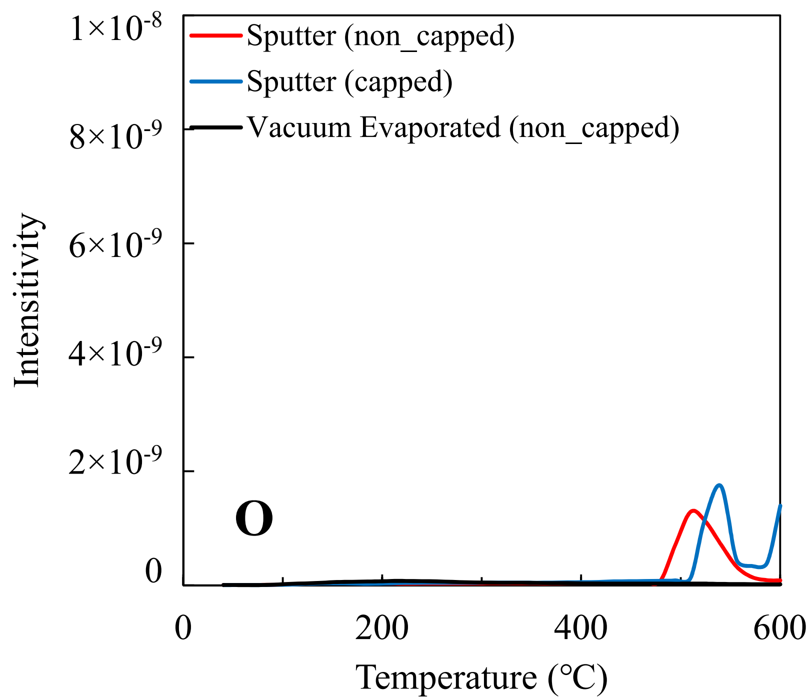

Fig. 5.8 (a) TDS results of InSb film for Oxygen gas (Conference Article [16]).

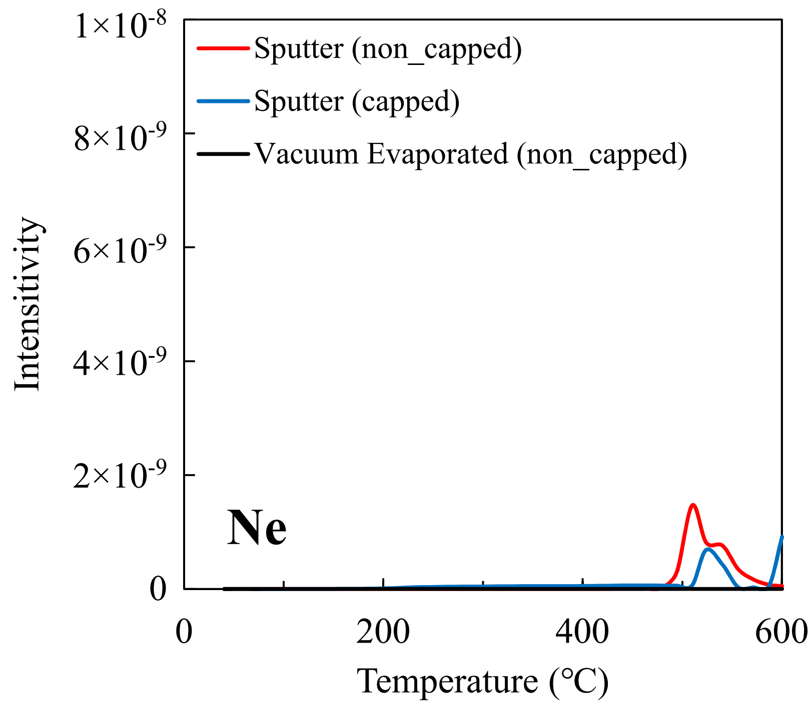

Fig. 5.8 (b) TDS results of InSb film for Ne gas (Conference Article [16]).

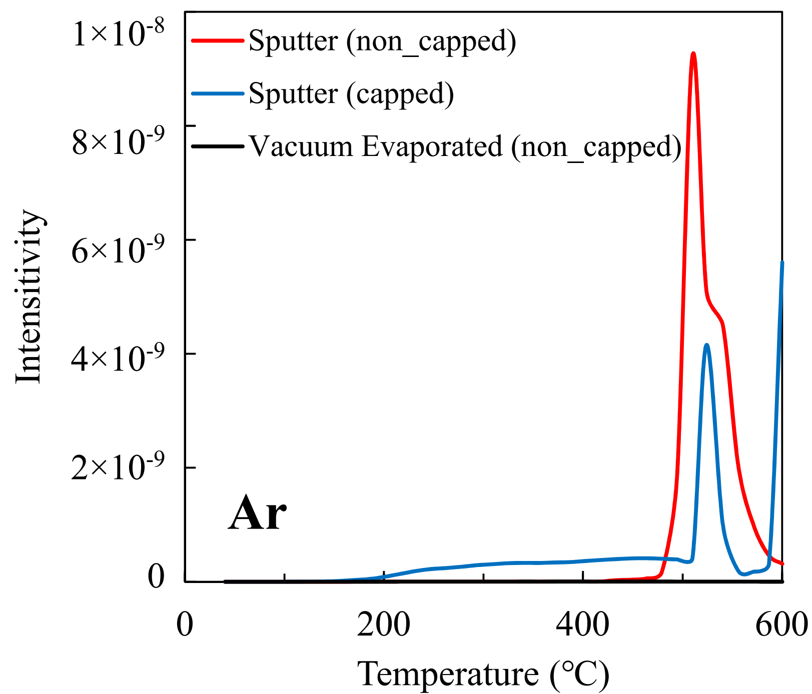

Fig. 5.8 (c) TDS results of InSb film for Ar gas (Conference Article [16]).

Fig. 5.9 shows the TDS results of InSb film for (a) In and (b) Sb. In or Sb was not released for both capped sputtered and thermal evaporated InSb films. However, Sb was released in the case of non-capped sputtered and thermal evaporated films. From Fig. 5.9 (b) shows that release of Sb started earlier (430°C) in the case of non-capped sputtered film than that of non-capped thermal evaporated film (480°C). This result suggests that extending the annealing time near 430°C may improve the crystallinity of sputtered InSb films by capping with SiO_2 or another material.

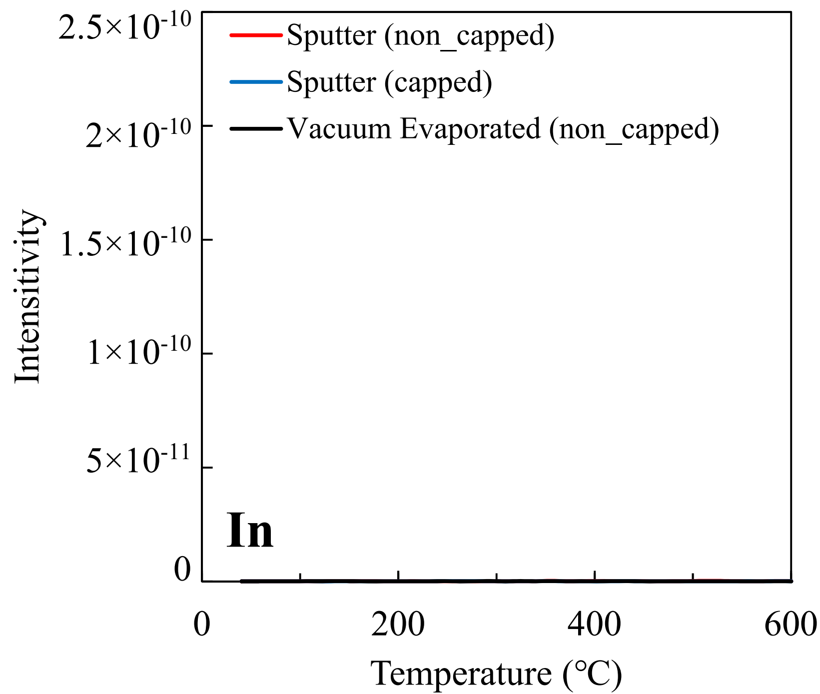

Fig. 5.9 (a) TDS results of InSb film for In (Conference Article [16]).

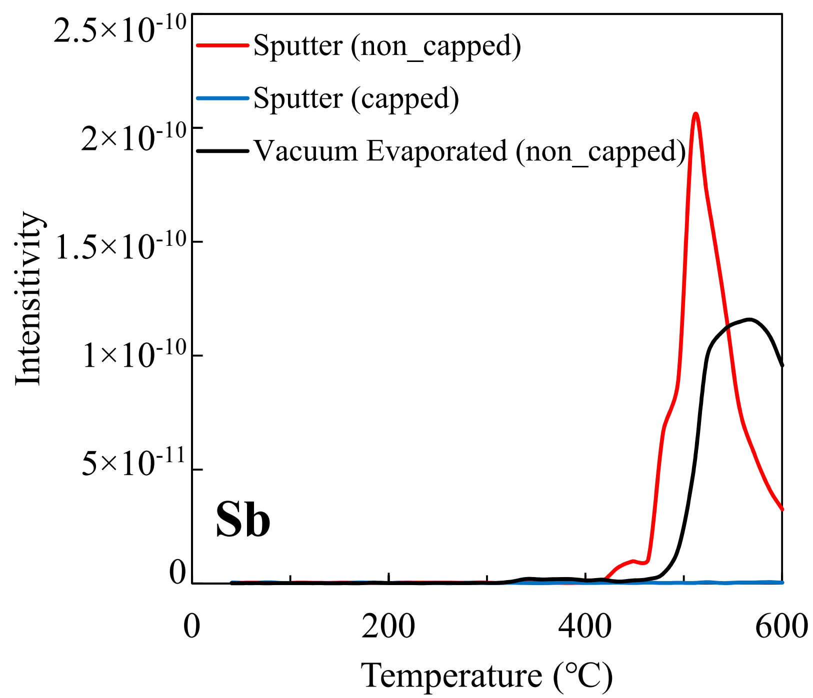

Fig. 5.9 (b) TDS results of InSb film for Sb (Conference Article [16]).

Chapter 6

Application as multifunctional TFT system on panel

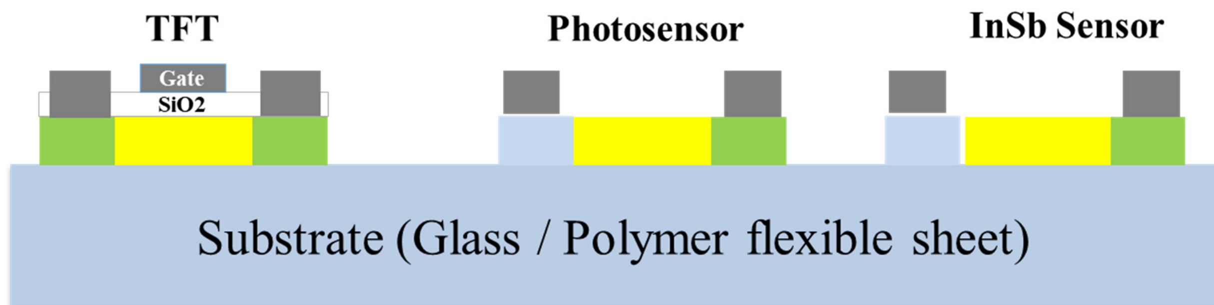

Fig. 6.1. Integrating sensor devices with TFTs on panel

Current trend for Internet on things (IoT) devices and new technology such as self-driving vehicles or multifunctional interactive displays is occurring a technology revolution. Specially in IoT and self-driving fields, enormous number of sensor devices are used. Therefore, semiconductor devices are also needed to be followed by inventing new ideas and applications.

Fig. 6.1 shows an example for system on panel (SoP) with TFTs integrated with InSb film (magnetic sensor) and photosensor devices. Product cost reduction, highly multi-functional devices can be achieved by integrating multiple sensor devices with TFTs circuits on panel. It is highly expected to deploy this kind of systems integrated with TFTs to functional sensors, high frequency band communication devices and optical communication panels.

Chapter 7

Summary and Conclusions

Effective crystallization process to realize advance multifunctional next generation System on Panel (SoP) which can integrate thin film Si photosensors or/and thin film InSb magnetic sensors with Thin Film Transistors (TFT) was investigated.

For thin amorphous Si (a-Si) film of 50 nm thickness fabricated using r.f. sputtering and the photoconductivity of poly-crystallized Si films after blue laser diode annealing (BLDA) has been measured and analyzed for photosensor applications. The crystal structure changed from micro grains to large grains with the increase of laser power. Photoconductivity value under the white light exposure of 100 mW/cm^2 reached as high as 8.1 x 10^{-4} S/cm for the Si film after the BLDA at 6 W and after subsequent H_2 annealing in H_2/N_2 (4%) ambient at 450°C. Resultant photosensitivity ratio ($\sigma_{photo}/\sigma_{dark}$) was 94. Simulation results showed 86% increase of light absorption in red or IR region by adopting back-reflection Ti layer under the Si film. X-Ray Diffraction (XRD) results showed that Si film was crystallized clearly after BLDA. Photoconductivity for the patterned Si films increased up from 1.2 x 10^{-4} to 3.2 x 10^{-1} S/cm under white light of 100 mW/cm^2 after H_2 annealing. These results suggest, adopting back-reflection layer under the crystallized Si film using BLDA is promising to integrate functional photosensors with TFTs on panel.

InSb films were deposited on both mica and glass substrates using thermal evaporation and subjected to FA or RTA. High value of electron Hall mobility as high as 25,000 cm^2/(Vs) was obtained with the capped InSb film by keeping the In:Sb ratio after RTA at 520°C for 30 sec or more without adopting epitaxial growth on glass. For the InSb films deposited using RF sputtering and Ne or Ar gases, RTA or BLDA was applied to crystallize the InSb films effectively. Electron Hall mobility of 1,650 cm^2/(Vs) was obtained after RTA at 500°C for 30 s. Maximum electron Hall mobility of 1,050 cm^2/(Vs) was obtained with the InSb film sputtered with Ar gas at the pressure of 7.0 mTorr for the sputtered InSb film of 300 nm thickness after BLDA at 4 W. These results suggest that both RTA and BLDA are promising candidate for crystallizing InSb film.

From the all above results, it is expected as magnetic sensor and other innovative applications such as SoG (System on Glass) or SoP (System on Panel) on flexible panels or sheets which is also applicable for future Internet on Things (IoT) devices.

Acknowledgements

I would like to acknowledge Professor Takashi Noguchi for the supervision, guidance and the great advices whole through from my undergraduate course to doctoral course. Also acknowledges the support and valuable comments from Professor Akira Higa at the University of the Ryukyus and Professor ByungSeong Bae at Hoseo University in South Korea, Assistant Professor Tatsuya Okada at the University of the Ryukyus.

Mr. Y. Ogino at Hitachi Information & Telecommunication Engineering, Ltd., Mr. K. Inoue and Mr. O. Baba and Mr. K. Yamada at Products Support Co., Ltd., Dr. T. Itoh and Dr. Y. Inoue of Corning Holding Japan G.K., Dr. T. Okuyama at TOYOBO, Mr. T. Kuroki at Ryukyu ALLCOM, Mr. S. Taniguchi, Mr. S. Yoshitome at e-tec Inc., Prof. M. Furuta, Mr. H. Tanaka of Kochi University of Technology, J. Sakuta and M. Tajima of Semilab Inc. and other co-researchers for support.

Mr. S. Chinen at Japan Display Inc. (previously in master course), Mr. K. Nakao at Sony Semiconductor Manufacturing Corporation (previously in master course), Mr. Higashizako Tatsuyuki at the University of the Ryukyus, Mr. S. Koyama at SIBATA Scientific Technology Ltd. for the encouragement.

Special thanks go to everyone in The Center for Research Advancement and Collaboration, International Student Center and Faculty of Engineering office of University of the Ryukyus.

This research was partially supported by the Strategic Core Technology Advancement Program of Japan, of Japan, Sangaku-kan-kin Collaborative Research Startup Support Project and thanks to Monbukagakusho scholarship sponsored by Ministry of Education, Culture, Sports, Science and Technology (MEXT), Japan.

List of Publications

Journal Publications

1. **C. J. Koswaththage**, S. Chinen, K. Sugihara, T. Okada and T. Noguchi, Photoconductivity of Si films after blue multi-laser diode annealing for photosensor applications, Jpn. J. Appl. Phys, vol. 53, (2014) 03CB02. DOI: 10.7567/JJAP.53.03CB02
2. **C. J. Koswaththage**, K. Nakao, T. Okada, T. Noguchi, Highly Photoconductive Si Film Formed by Blue Laser Diode Annealing for System on Panel, Journal of Display Technology, Volume 12, Issue 3 (2016) pp.247-251. DOI: 10.1109/JDT.2015.2463116
3. **C. J. Koswaththage**, T. Okada, T. Noguchi, S. Taniguchi, and S. Yoshitome, Ultra-high carrier mobility InSb film by rapid thermal annealing on glass substrate, AIP Advances, Volume 6, Issue 11 (2016) 115303. DOI: 10.1063/1.4967287

International Conferences

1. S. Chinen, **C. J. Koswaththage**, K. Sugihara, T. Okada, T. Noguchi, ChangMin Keum, B.S. Bae, and T. Ohachi, Advanced Si Photo-Sensor in TFT System for FPD by BLDA, The 9th International Thin-Film Transistor Conference (Tokyo, March 1-2, 2013) p.44 [1pLP08].
2. **C. J. Koswaththage**, S. Chinen, K. Sugihara, T. Okada and T. Noguchi, Thin Film Photo-Sensor by BLDA to Realize System on Panel, International Workshop On Active-Matrix Flatpanel Displays And Devices (Kyoto, July 4-7, 2013) pp.141-142 [P-L2]
3. T. Noguchi, K. Shimoda, K. Sugihara, **C. J. Koswaththage**, S. Chinen And T. Okada, Advanced Crystallization of Si Films on Panel using Blue Laser-Diode, 10th International Thin-Film Transistor Conference (Delft, The Netherlands, January 23-24, 2014) p.13.
4. K. Nakao, **C. J. Koswaththage**, T. Okada, T. Noguchi, Remarkable Increase in Photoconductivity of Patterned Poly-Si Thin Films by BLDA for System on Glass, The 14th International Meeting on Information Display (Daegu, Korea, August 26-29, 2014) [P1-47].
5. K. Sugihara, K. Shimoda, K. Imura, T. Ashitomi, **C. J. Koswaththage**, T. Okada And T. Noguchi, Advanced Low-Temperature Poly Si TFTs without Impurity Doping using BLDA (Blue Multi-Laser Diode Annealing) , 2014 Asia-Pacific Workshop on Fundamentals and Applications of Advanced Semiconductor Devices (Kanazawa, July 1-3, 2014) pp.122-124 [3A-3].
6. T. Noguchi, K. Shimoda, T. Ashitomi, **C. J. Koswaththage**, K. Nakao and T. Okada, Low cost TFT Process for LTPS, The 10th International Display Valley Conference & Exhibition (Asan, Krea, November 11-13, 2014) pp.19.

7. **C. J. Koswaththage**, K. Nakao, T. Okada, and T. Noguchi, Highly Photoconductive Si film Formed by Blue-Multi Laser Diode Annealing for System on Panel, 11th International Thin-Film Transistor Conference (Rennes, France, February 26-27, 2015) pp.93-94.
8. T. Noguchi, K. Shimoda, T. Ashitomi, K. Nakao, **C. J. Koswaththage**, and T. Okada, Low-Cost LTPS Using Blue Laser Diode Annealing, 11th International Thin-Film Transistor Conference (Rennes, France, February 26-27, 2015) pp.191-192.
9. K. Nakao, **C. J. Koswaththage**, T. Okada and T. Noguchi, Increase in Photoconductivity of Silicon Films after BLDA by Back-Reflection Ti Layer for System on Glass, The 15th International Meeting on Information Display (Daegu, Korea, August 18-21, 2015) p.467 [P2-39].
10. T. Noguchi, Takuya Ashitomi, Kiyoharu Shimoda, Kimihiko Imura, Kota Nakao, **C. J. Koswaththage** and T. Okada, New Laser Crystallization for LTPS on Panel, The 15th International Meeting on Information Display (Daegu, Korea, August 18-21, 2015) pp.121-122 [29-1].
11. T. Ashitomi, T. Harada, K. Nakao, **C. J. Koswaththage**, T. Okada, T. Noguchi, N. Kawamoto, H. Ikenoue, T. Okuyama, A. Suwa, and K. Noda, Stable Crystallization of a-Si Film on a Flexible Substrate, Proc. of the 22nd International Display Workshops (Otsu Prince Hotel, Otsu, December 9-11, 2015) pp.1405-1406 [FLXp1-7L].
12. T. Higashizako, **C. J. Koswththage**, K. Nakao, T. Okada, and T. Noguchi, Photoelectric Characteristics of Lateral Thin Film Si Photodiode by Metal Electrodes for SoP, The 16th International Meeting on Information Display (Jeju, Korea, August 23-26, 2016) p.236 [D52-3].
13. **C. J. Koswaththage**, T. Okada, S. Taniguchi, S. Yoshitome, and T. Noguchi, Ultra-high Carrier Mobility InSb Film by Rapid Thermal Annealing for Advanced Sensor Applications on Glass, 13th International Thin-Film Transistor Conference (Austin, Tx, USA, February 23-24, 2017) pp.31-32.
14. **C.J. Koswaththage**, T. Higashizako, T. Okada, and T. Noguchi, Sputtered InSb film after RTA for Magnetic Sensor Applications, The 17th International Meeting on Information Display (BEXCO, Busan, Korea, August 28-31, 2017) [D36-4].
15. **C. J. Koswaththage**, T. Harada, F. Gakiya, T. Higashizako, Y. Ishiki, T. Okada and T. Okada, High mobility InSb film with poly-Si TFTs formed by Laser Annealing for Flexible Advanced System on Polymer, The 24th International Display Workshops (Sendai, December 6-8, 2017).
16. **C. J. Koswaththage,** T. Higashizako, T. Okada and T. Noguchi, Electron Hall Mobility of Ne and Ar Sputtered InSb films for Advanced Sensor Applications on Glass, 14th International Thin-Film Transistor Conference (Guangzhou, China, February 28 – March 2, 2018).

Domestic Conferences (Japan)

1. **C. J. Koswaththage**, S. Chinen, T. Mukae, K. Sugihara, T. Okada and T. Noguchi, Simulation analysis to improve the photo-current of PIN diode sensor with back-reflection film, 平成 24 年度　琉大工学部・沖縄高専学生研究発表交流, 2013 年 1 月 24 日
2. K. Nakao, S. Chinen, **C. J. Koswaththage**, T. Okada, T. Noguchi, 2 ステップ熱アニールを施した poly-Si フォトセンサの作製, 平成 25 年度 電気学会九州支部沖縄支所講演会 (琉球大学, 2013 年 12 月 7 日) pp.111-114 [OKI-2013-28].
3. **C. J. Koswaththage**, S. Chinen, K. Sugihara, T. Okada, and T. Noguchi, Photoconductivity of Si Films on glass after Blue Multi-Laser Diode Annealing, SDM シリコン材料・デバイス研究会 (2014 年 4 月 10-11 日) pp.63-65 [SDM2014-15(OME2014-15)].
4. **C. J. Koswaththage**, K. Nakao, T. Okada, and T. Noguchi, 微細化した Si 膜の BLDA (Blue Laser Diode Annealing) による電気特性の向上, 平成 26 年度 電気学会九州支部沖縄支所講演会 (琉球大学, 2014 年 11 月 29 日) pp.27-29 [OKI-2014-09].
5. **C. J. Koswaththage**, T. Noguchi, S. Taniguchi, and S. Yoshitome, Thermal annealing of Thin Film InSb on Mica and Glass Substrate, The 62nd JSAP Spring Meeting (Tokai University, March 11-14, 2015) p.13-276 [13p-D4-11].
6. K. Nakao, **C. J. Koswaththage**, T. Wakasugi, T. Okada, and T. Noguchi, Improved Crystallinity of Si Film after BLDA for Photosensor of Multi-Layer Film Structure, The 62nd JSAP Spring Meeting (Tokai University, March 11-14, 2015) p.12-184 [12a-A29-8].
7. **C.J. Koswaththage**, K. Nakao, K. Koyama, T. Okada, T. Noguchi, Photosensitivity of Ge Film after Furnace Annealing, JSAP Kyushu Chapter Annual Meeting 2015 (Univ. Ryukyus, December 5-6, 2015) p.88 [5Da-9].
8. T. Ashitomi, T. Harada, K. Nakao, **C. J. Koswaththage**, T. Okada, T. Noguchi, N. Kawamoto, H. Ikenoue, T. Okuyama, A. Suwa, K. Noda, Stable Crystallization of a-Si Film on a Flexible Substrate, Proc. of IDW 15, FLXp1-7L, p. 1405, 2015 (Otsu, Japan).
9. T. Higashizako, **C. J. Koswaththage**, K. Nakao, T. Okada, and T. Noguchi, Title, 平成 27 年度 電気学会九州支部沖縄支所講演会 (琉球大学, 2015 年 12 月 19 日) pp.36-38 [OKI-2015-13].
10. S. Koyama, **C. J. Koswaththage**, K. Nakao, T. Okada, and T. Noguchi, Title, 平成 27 年度 電気学会九州支部沖縄支所講演会 (琉球大学, 2015 年 12 月 19 日) pp.33-35 [OKI-2015-12].
11. **C. J. Koswaththage**, T. Noguchi, S. Taniguchi, and S. Yoshitome, Electrical characteristics of rapid heat-treated InSb film, The 63rd JSAP Spring Meeting (Tokyo Inst. of Tech., March 19-22, 2016) p.12_243 [21p-H112-13].

12. **C. J. Koswaththage**, K. Nakao, T. Okada, and T. Noguchi, High Photoconductive Silicon Thin-film formed by Blue Laser Diode Annealing for System on Panel, SDM シリコン材料・デバイス研究会 (2016 年 4 月 8-9 日) pp.43-47 [SDM2016-11, OME2016-11].
13. M. Oota, **C. J. Koswaththage**, T. Higashizako, T. Okada and T. Noguchi, Evaluation of crystalline and electrical properties of Ge thin film subjected to rapid thermal annealing, 平成 28 年度 電気学会九州支部沖縄支所講演会 (琉球大学, 2016 年 12 月 11 日) [OKI-2016-48].
14. T. Higashizako, **C. J. Koswaththage**, T. Okada and T. Noguchi, Effect of Hydrogen annealing on BLDA applied Si thin films, 平成 28 年度 電気学会九州支部沖縄支所講演会 (琉球大学, 2016 年 12 月 11 日) [OKI-2016-46].
15. **C. J. Koswaththage**, T. Higashizako, T. Okada and T. Noguchi, Electrical characteristics of InSb films after BLDA, The 78th JSAP Autumn Meeting (Fukuoka International Congress Center, September 5-8, 2017)
16. H. Sugiyama, **C. J. Koswaththage**, T. Higashizako, T. Okada and T. Noguchi, Solid phase crystallization of Si thin film using RTA, Records of 2017 Conference of IEEJ in Okinawa (University of the Ryukyus, December 10, 2017) [OKI-2017-38].
17. **C. J. Koswaththage**, T. Higashizako, T. Okada, T. Noguchi, H. Tanaka and M. Furuta, Capping Effect of Crystallized InSb film on Glass, The 65th JSAP Spring Meeting (Waseda University, March 17 – 20, 2018) (to be presented)

Academic Awards

1. Graduation Research Presentation Excellence Award, Department of Electrical and Electronic Engineering, Faculty of Engineering, University of the Ryukyus (March 2013)
2. Winner of the 2016 Excellent Student Award of IEEE Fukuoka Section (February 2017)

Patents

1. 野口　隆、岡田　竜弥、安次富　卓也、コスワッタゲー　チャリット　ジャヤナダ、中尾浩太（特願 2015-239619）

Research Experiance

1. InSb を用いた高感度磁気センサーに関する研究, e-tec INC 社との共同研究 (2013)